Materials and methods

Chemicals and solutions. High-performance liquid chromatography (HPLC)-grade methanol and formic acid were purchased from Kanto Chemical (Tokyo, Japan). 5-FU was purchased from Kyowa Hakko (Tokyo, Japan).

Cell culture and treatment. Human poorly differentiated gastric adenocarcinoma MKN45 cells were purchased from the American Type Culture Collection and maintained in RPMI-1640 medium, supplemented with 10% fetal bovine serum, 100 U/ml penicillin, and 100 μg/ml streptomycin in a humidified atmosphere of 5% CO_2 at 37˚C. 5-FU-resistant MKN45/F2R cells were maintained in a culture medium containing 2 μM 5-FU. To eliminate the effects of 5-FU in our experiments, the resistant cells were cultured in a drug-free medium for at least 2 weeks before any procedure. Each cell line was planted in 6-well plates at a density of $1x10^6$ per well. Cells were exposed to 10 μM 5-FU or medium alone (control group, 0 h). At specified times (up to 12 h after the onset of treatment), cells were rinsed 3 times with phosphate-buffered saline (PBS) and harvested by trypsinization.

Cell proliferation assay. Gastric cancer cells were seeded onto 96-well plates ($1x10^4$ cells/well). After 24 h, the cells were treated with various concentrations of 5-FU in 100 μl medium and incubated at 37˚C in an atmosphere of 5% CO_2. After the 72-h incubation period, CellTiter 96® Aqueous One Solution (Promega, Madison, WI, USA) was added (20 μl/well) and the resultant mixture was incubated for 1 h at 37˚C in an atmosphere of 5% CO_2. Then, the absorbance at 490 nm with a reference at 650 nm was measured with an Emax microplate reader (Molecular Devices, Tokyo, Japan).

LC-MS. Harvested cells were transferred to a 1.5-ml conical tube and spun down. Cells were then washed with PBS once. Excess PBS was removed by aspiration, and the cell pellets were suspended in methanol (100 μl/10^6 cells), followed by sonication. The samples were then centrifuged at 10,000 x g at 4˚C for 10 min, and supernatants were dispensed and stocked at -40˚C.

For LC separation, a binary gradient HPLC system consisting of an LC-20AD pump coupled to an SIL-20AC autosampler (Shimadzu, Kyoto, Japan) with the sample cooler set at 4˚C was used. Chromatographic reversed-phase separations were performed on an L-column2 ODS (1.5x150 mm, 5 μm) (CERI, Tokyo, Japan), operated at room temperature. The mobile phases used consisted of purified water containing 0.1% formic acid as solvent A, and methanol containing 0.1% formic acid as solvent B. The flow-rate gradient and buffer composition were produced as follows: 0-1 min, held at 3% solvent B using a flow rate of 60 μl/min; 1-3 min, linear flow rate gradient from 60 to 20 μl/min; 3-6 min, held at 20 μl/min; 6-16 min, linear gradient of buffer composition from 3 to 99% solvent B and of flow rate from 20 to 60 μl/min; 16-45 min, held at 99% solvent B; 45-57 min, back to 3% solvent B and re-equilibrated for 12 min using a flow rate of 170 μl/min.

Mass spectrometry experiments were carried out on a QSTAR Elite, a hybrid quadrupole time-of-flight instrument attached to a Turboionspray electrospray ionization source (AB SCIEX, Framingham, MA, USA) working on positive-ion mode. The LC eluate was ionized at a spray voltage of 4.5 kV. We used information-dependent acquisition in data-acquisition software Analyst QS to obtain both full-scan spectra of *m/z* 50-1000 and MS/MS spectra of automatically detected peaks. Then, mass spectra were analyzed using Marker View software version 1.2 (AB SCIEX) to perform peak extraction, data alignment with LC retention time, normalization by total peak area, and statistical analyses.

Reverse transcription-polymerase chain reaction (RT-PCR). Total RNA was isolated using an RNeasy Mini kit (Qiagen, Chatsworth, CA, USA) and reverse transcribed with a Transcriptor First-Strand cDNA Synthesis kit (Roche, Tokyo, Japan). PCRs were performed with KOD FX (Toyobo, Osaka, Japan) and GeneAmp PCR System 9700 (Applied Biosystems, Tokyo, Japan). The specific primers for PRODH were: forward, 5'-CGGAGAGCAGGAGCAGAGGCTTTGA-3'; reverse, 5'-GCCGTGGACAGCGGGACGAA-3'. Glyceraldehyde-3-phosphate dehydrogenase (GAPDH) was amplified as a loading control with the following primers: forward, 5'-ACCA CAGTCCATGCCATCAC-3'; reverse, 5'-TCCACCACCC TGTTGCTGTA-3'. The PCR profile was 94˚C for 2 min, 35 cycles at 98˚C for 10 sec, 60˚C for 30 sec, and 68˚C for 30 sec. All reaction products (10 μl with glycerol loading buffer) were run on a 1% agarose gel and stained with ethidium bromide. Data were normalized to GAPDH.

Reactive oxygen species (ROS)/superoxide measurement. To measure intracellular ROS and superoxide, a Total ROS/Superoxide detection kit (Enzo Life Sciences, Farmingdale, NY, USA) was used. Cells were stained for 30 min at 37˚C in the dark with 1 μM of ROS and superoxide-sensitive fluorescent dyes, and subsequently assayed by flow cytometry FACSAria II (BD Biosciences, San Jose, CA, USA). Double staining with fluorescein isothiocyanate and phycoerythrin was carried out, and data were assessed by FlowJo software version 7.6 (Tomy Digital Biology Co., Tokyo, Japan).

Statistical analyses. Data for metabolites and mRNA expression were calculated and expressed as the mean ± standard deviation (SD) from at least 3 experiments. Statistical analysis of LC-MS data on Marker View 1.2 consisted of principal component analysis (PCA) with Pareto scaling and Student's t-test. For the mRNA experiments, a t-test was performed using Microsoft Excel.

Results

Drug sensitivity of gastric cancer cell lines. MKN45/F2R cells were more resistant to 5-FU than were MKN45 cells (Fig. 1). The IC_{50} of MKN45 and MKN45/F2R cells were 23.8 and 161 μM, respectively. Growth in the absence of 5-FU was not appreciably different between the 2 cell lines (data not shown). In subsequent experiments, a drug concentration of 10 μM was used to examine the effects of a larger difference.

Metabolome analysis. The LC-MS analysis yielded the raw data, detecting 7107 (MKN45) and 5696 (MKN45/F2R) peaks. Among these, the numbers of peaks that increased by more

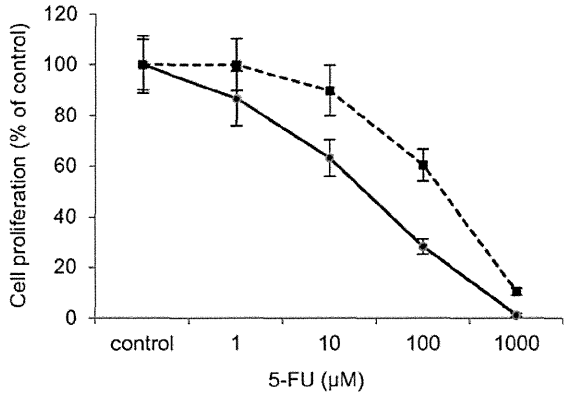

Figure 1. *In vivo* sensitivity of MKN45 (●) and MKN45/F2R (■) cells to 5-FU. Cells were cultured with various concentrations of 5-FU for 72 h. The relative number of living cells was measured, with each data point representing the mean ± SD.

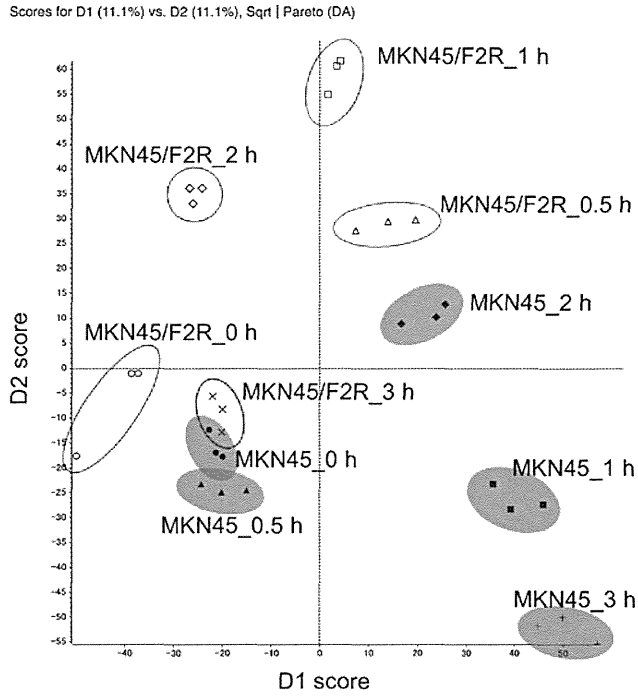

Figure 2. Scores plot from PCA of LC-MS data for MKN45 and MKN45/F2R cells. Each time-period group was separated from the other groups. Gray circles, MKN45 cells; void circles, MKN45/F2R cells.

than double their original size after 5-FU treatment were 642 (MKN45) and 140 (MKN45/F2R), and the numbers of peaks that decreased to less than half of their original size were 285 (MKN45) and 18 (MKN45/F2R). The identified metabolites are listed in Table I. Most of the peaks were identified as endogenous metabolites, such as amino acids, organic acids, lipids, and purines. To determine whether these spectra contained unique peaks that could differentiate the metabolic responses of the 2 cell lines, PCA was performed (Fig. 2). Each treatment-period group was clustered and separated from other groups, and the resultant data indicated the characteristic metabolic profiles of the cellular responses to 5-FU.

We then attempted to identify the responsible molecules that could serve as markers for 5-FU response. For those differential molecules, a time course validation of major amino acids is shown in Fig. 3. We found that the fluctuation for MKN45/F2R was less than that for MKN45 cells. In MKN45, the amino acids increasing at 3 h were glutamate, methionine and arginine, while those decreasing at 3 h were proline, valine, asparagine and citrulline. The transiently altered amino acids were oxoproline and aspartate. On the other hand, in MKN45/F2R cells, only glutamate increased at 3 h. In particular, proline and glutamate were very abundant and closely related in this metabolic pathway. In MKN45 cells, proline was reduced to one-third of its original value, and glutamate was increased to 3 times its original value after 3 h of treatment. These results suggest that the metabolic enzymes associated with the differential metabolites played an important role in the response to treatment and may be behind the mechanism of resistance to 5-FU. Among these enzymes, PRODH is particularly important; it catalyzes the first and the rate-limiting step of 2 reactions converting proline to glutamate at the mitochondria, and the catabolism of proline produces superoxide.

Upregulation of PRODH mRNA and ROS/superoxide generation after 5-FU treatment. We then investigated the amount that PRODH gene expression was altered in response to 5-FU stimulation. A significant increase in the concentration of PRODH mRNA was observed in MKN45 cells after 6 h of treatment (Fig. 4). The expression of PRODH mRNA peaked after 6 h of treatment, resulting in a 2-fold increase in the PRODH transcript level. In MKN45/F2R cells, PRODH mRNA expression did not vary over time.

In general, proline catabolism first produces a superoxide anion with the chemical formula O_2^-, which is subsequently changed into a variety of ROS. Therefore, we not only highlighted ROS, but also superoxide. We found that both MKN45 and MKN45/F2R cells produced more superoxide than ROS, and MKN45/F2R produced more superoxide than MKN45 at the baseline. In MKN45 cells, the shift to the upper left quadrant was recognized, indicating the increased superoxide generation. In MKN45 cells, the mean fluorescence intensity of superoxide increased 3-fold following 3 h of treatment, while in MKN45/F2R, the intensity did not increase (Fig. 5).

Discussion

In this study, we focused on small-molecule metabolites to investigate the characteristics of cancer cells and the cellular response to 5-FU. While there have been some metabolomic reports on the comparison between cancer and normal tissue (13), cancer metastasis (14), and the cancer response to chemotherapy (9-11), to our knowledge, this is the first metabolomics-based study of the short-term, cellular, dynamic response of gastric cancer cells and the resistance mechanisms to an anticancer agent.

A previous study proposed a metabolic workflow for the LC-MS/MS platform (15). In this scheme, the first step is sample handling, followed by analytical treatment, quality assessment and multivariate analysis, data reduction by principal component variable grouping and groups interpretation, listing of candidates (biomarkers), and finally, biomarker identification. We followed virtually the same workflow with our method. Candidates were searched in the metabolomics database

Table I. Metabolites identified from gastric cancer cells by LC-MS/MS study.

Molecule	Formula	*m/z*	RT (min)	MS fragments *(m/z)*
Glycine	$C_2H_5NO_2$	76.04	6.09	
Alanine	$C_3H_7NO_2$	90.05	6.23	
Serine	$C_3H_7NO_3$	106.05	6.16	60
Creatinine	$C_4H_7N_3O$	114.07	5.7	
Proline	$C_5H_9NO_2$	116.07	6.64	70
Guanidinoacetate	$C_3H_7N_3O_2$	118.06	6.06	72, 76, 101
Valine	$C_5H_{11}NO_2$	118.09	6.6	72
Threonine	$C_4H_9NO_3$	120.07	6.31	56, 74, 102
Cysteine	$C_3H_7NO_2S$	122.03	6.43	76
Oxoproline	$C_5H_7NO_3$	130.05	6.42	84
Creatine	$C_4H_9N_3O_2$	132.08	6.36	90
Leucine/Isoleucine	$C_6H_{13}NO_2$	132.10	11.22	86
Asparagine	$C_4H_8N_2O_3$	133.06	6.45	74, 87, 116
Aspartate	$C_4H_7NO_4$	134.04	6.57	70, 74, 88
Adenine	$C_5H_5N_5$	136.06	6.6	81, 119
4-Guanidinobutanoate	$C_5H_{11}N_3O_2$	146.09	6.48	
γ-Butyrobetaine	$C_7H_{15}NO_2$	146.11	5.7	60, 87
Glutamine	$C_5H_{10}N_2O_3$	147.08	6.25	84, 130
Glutamate	$C_5H_9NO_4$	148.06	6.4	84, 102, 130
Methionine	$C_5H_{11}NO_2S$	150.06	8.76	104, 133
Histidine	$C_6H_9N_3O_2$	156.08	5.67	110
Carnitine	$C_7H_{15}NO_3$	162.11	5.7	60, 85, 103
Phenylalanine	$C_9H_{11}NO_2$	166.09	18.47	120
Arginine	$C_6H_{14}N_4O_2$	175.12	5.71	60, 70, 116, 130, 158
Citrulline	$C_6H_{13}N_3O_3$	176.10	6.26	70, 113, 159
Tyrosine	$C_9H_{11}NO_3$	182.08	11.53	136, 165
Phosphocholine	$C_5H_{15}NO_4P$	184.07	6.24	86, 125
Glucose	$C_6H_{12}O_6$	203.05	6.08	
Acetylcarnitine	$C_9H_{18}NO_4$	204.12	6.62	85, 145
Propionylcarnitine	$C_{10}H_{19}NO_4$	218.13	6.74	85, 159
Pantothenate	$C_9H_{17}NO_5$	220.12	26.68	72, 90, 202
Lumichrome	$C_{12}H_{10}N_4O_2$	243.09	31.87	172, 198
L-Argininosuccinate	$C_{10}H_{18}N_4O_6$	291.13	6.28	
5'-Methylthioadenosine	$C_{11}H_{15}N_5O_3S$	298.10	28.11	136
Ketosphingosine	$C_{18}H_{35}NO_2$	298.27	33.07	282
Sphingosine	$C_{18}H_{37}NO_2$	300.29	33.67	252, 282
Sphinganine	$C_{18}H_{39}NO_2$	302.31	33.97	
Glutathione	$C_{10}H_{17}N_3O_6S$	308.09	9.98	179
N-Acetylneuraminate	$C_{11}H_{19}NO_9$	310.11	8.76	121, 167, 274, 292
Phytosphingosine	$C_{18}H_{39}NO_3$	318.30	33.6	282
Palmitoylcarnitine	$C_{23}H_{45}NO_4$	400.34	35.55	85

m/z, mass to charge ratio; RT, retention time; MS, mass spectrometry.

KEGG (16), and MS/MS spectral searches were carried out on MassBank (17). Since even mass accuracy below 1 ppm would generate large lists of potential biomarkers, further MS/MS data were mandatory for structural confirmation. In general, multivariate analysis plays a key role in metabolomics for the comparison of large sets of data from various samples. In the case of LC-MS, metabolomics data processing generates a large amount of features consisting of retention time and *m/z*. Pattern

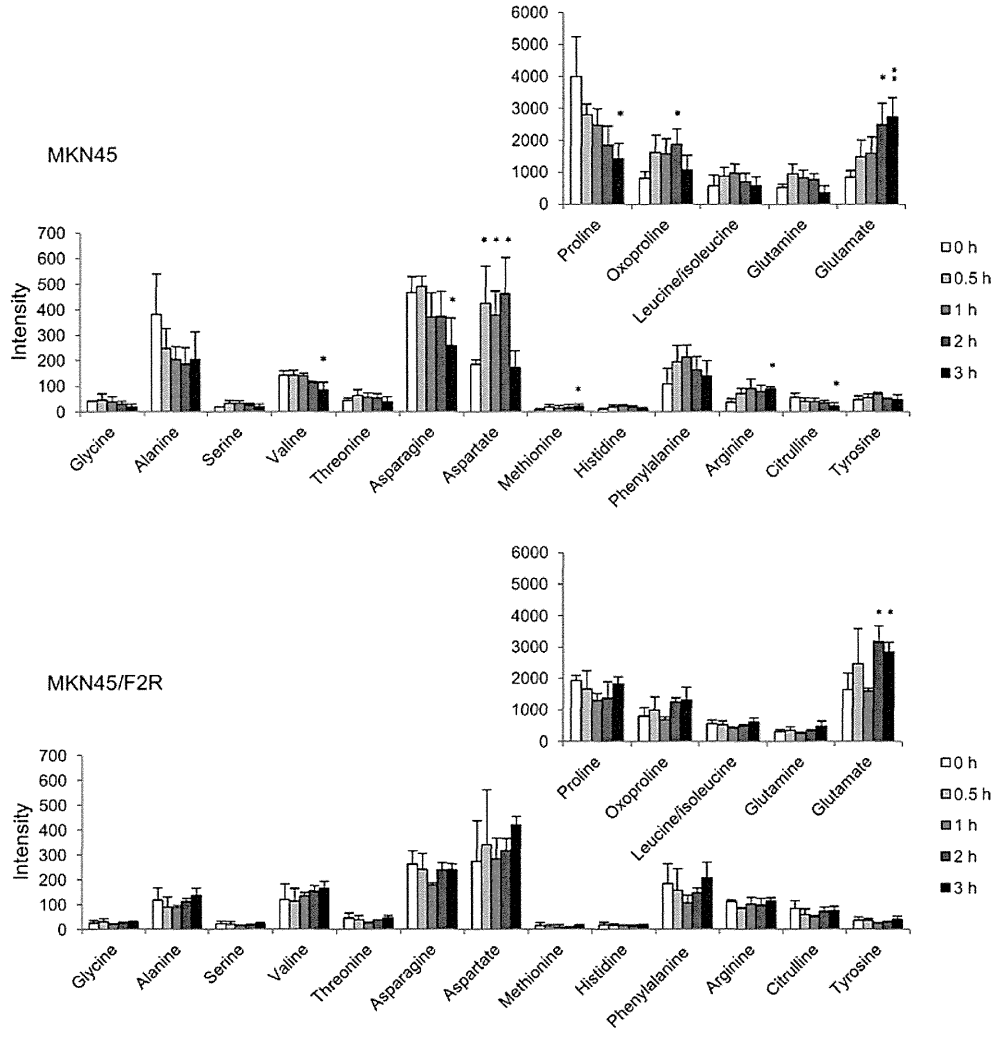

Figure 3. Metabolite profiling of MKN45 and MKN45/F2R cells. Time course validation of major amino acids was measured by LC-MS analysis, with each data point representing the mean ± SD. *P<0.05; **P<0.01 are for comparison of 5-FU-treated cells vs. untreated cells.

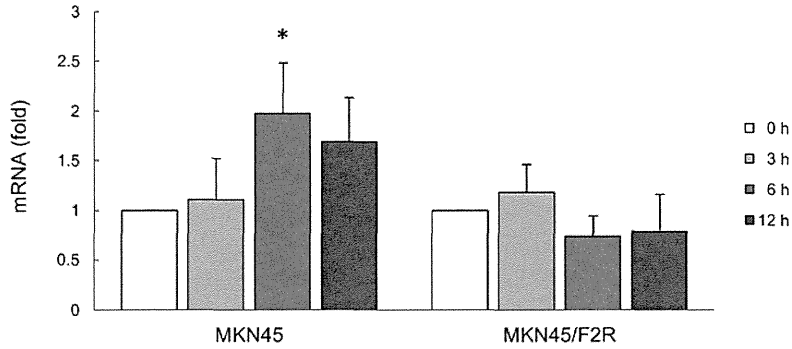

Figure 4. The fluctuation of PRODH mRNA expression levels in response to 5-FU stimulation was measured by RT-PCR. The graphs show the densitometric analysis of the relative expression of PRODH mRNA normalized to GAPDH. *P<0.05 is for comparison of 5-FU-treated cells vs. untreated cells.

recognition tools, such as PCA, show covariation between metabolites, with metabolism global trends retaining the largest part of the information (18).

Previously, researchers have focused more on cancer metabolism because of the realization that cancer genomics can be understood on the basis of metabolic pathways (19,20). However, little attention has been given to amino acids as substrate for energetics or as mediators of cellular signaling (21). Tumor cells require large amounts of nutrients, including amino acids, for rapid growth and uncontrolled proliferation, leading to perturbations in the amino acid metabolism of cancer (22).

In this study, the intracellular metabolites of gastric cancer cells dynamically changed within a few hours following 5-FU

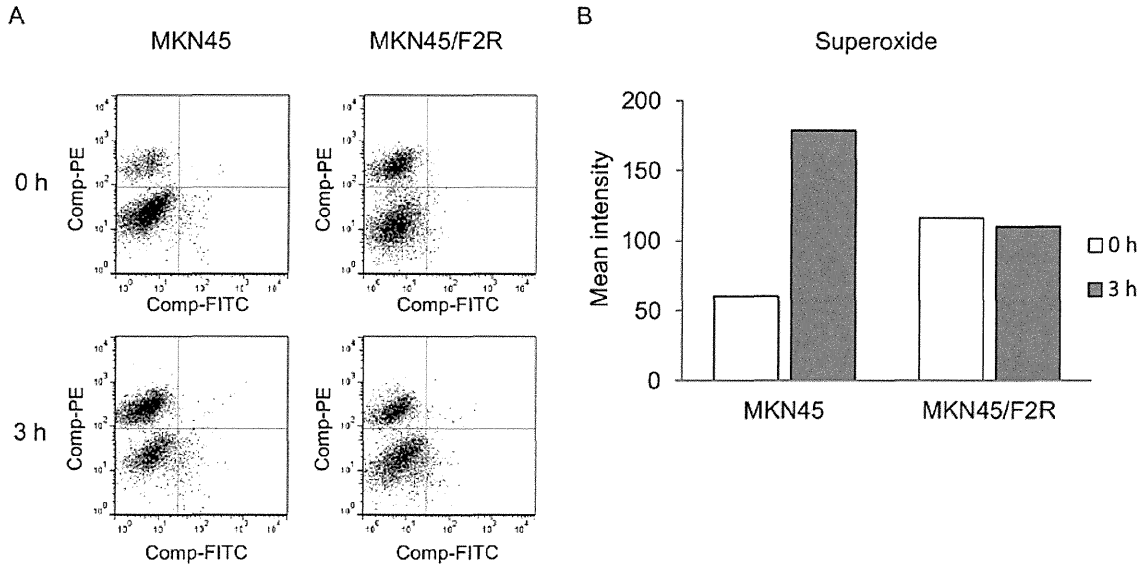

Figure 5. ROS/superoxide assay by flow cytometry. (A) ROS was measured with fluorescein isothiocyanate (FITC) and superoxide with phycoerythrin (PE). Significant numbers of superoxide-producing cells were observed in the MKN45 cells following 5-FU treatment. (B) The mean fluorescence intensity of superoxide in MKN45 and MKN45/F2R cells is shown in the histogram.

treatment. In particular, several amino acids were dramatically up or downregulated. Among these, we highlighted 2, proline and glutamate, since they were abundant and were continuously altered in MKN45 cells following 5-FU treatment. Additionally, the percentage of amino acids in the medium remained virtually unchanged after treatment (data not shown). This indicates that both proline and glutamate were metabolized within cells instead of being taken up into cells.

We additionally analyzed the molecule PRODH, also known as proline oxidase, a mitochondrial inner membrane enzyme that catalyzes the first step of proline degradation (23). In this process, proline is converted to glutamate through an intermediate, pyrroline-5-carboxylate (P5C). The function of PRODH is to catalyze the rate-limiting, 2-electron oxidation of proline to P5C, and the pair of electrons can then be used for direct reduction of oxygen to form superoxide (24). The superoxide is then transformed to ROS, a molecule related to cell death. PRODH has been found to be upregulated by p53, peroxisomal proliferator-activated receptor γ, and metabolic stress (21,25,26). Although PRODH expression levels were found to be much lower in several types of cancers, including stomach cancer, as compared to normal tissues (27), the relationship between PRODH and the anticancer effect of 5-FU has yet to be elucidated.

The present study demonstrated the upregulation of PRODH mRNA expression and superoxide generation in the gastric cancer cell line MKN45 following 5-FU treatment. This result indicates that 5-FU induces the PRODH gene directly or indirectly and stimulates the generation of mitochondrial superoxide, following cell death. In fact, PRODH mRNA expression was slower than the production of superoxide. In one potential explanation for these results, PRODH activity might first be stimulated by 5-FU, and the secondary gene expression might then be induced. The PRODH enzyme activity may be expressed as the ratio of proline to P5C. However, in this study, P5C could not be fully detected. The explanation for this result was thought to be that P5C was present at too small levels to be detectable or that it was an acidic substance. Thus, more sensitive measurements or the negative ion mode assay may be necessary.

Another mechanism of cell death may involve hypoxia-inducible factor-1α (HIF-1α) and vascular endothelial growth factor (VEGF) (21,27). PRODH produces P5C, which can then be converted to glutamate and α-ketoglutarate (α-KG). Since α-KG is not only a central substrate of the tricarboxylic acid cycle, but also a critical substrate for prolyl hydroxylase (PHD), HIF-1α may be downregulated by PHD activity. The expression levels of HIF-1α and its downstream gene, VEGF, have been shown to be reduced by PRODH (27).

We also investigated the mechanism of resistance to 5-FU using 5-FU-resistant cells. Specifically, we studied MKN45/F2R, which is a 5-FU-resistant cell line derived from MKN45 gastric cancer cells (12). The decrease in orotate phosphoribosyltransferase (OPRT), which metabolizes 5-FU to 5-fluorouridine monophosphate, plays an important role in the resistance to 5-FU chemotherapy (12). However, MKN45/F2R cells show cross-resistance to other agents, such as taxanes, platinum agents and SN38. In addition, OPRT-knockout MKN45 cells were found to be more resistant than were MKN45 cells (12). This indicates that other factors correlate with drug resistance. Although several candidate genes were identified, the mechanism of resistance is not well known. In the current metabolome analysis, fewer amino acids in MKN45/F2R cells showed change than in MKN45 cells following 5-FU treatment. This lower rate of effect can be traced to drug resistance. Since PRODH mRNA expression and superoxide generation in MKN45/F2R cells were not upregulated following 5-FU treatment, we can conclude that PRODH may be involved in drug resistance. The present study suggests that the inhibition of DNA or RNA synthesis by 5-FU and the resultant genetic stress induces PRODH activity following mitochondrial superoxide generation, represented as changes in metabolites.

The metabolomics approach to cancer research is still in a challenging phase despite advances in metabolomic techniques used in various scientific fields. We performed a metabolomic analysis of the effect of 5-FU treatment on human gastric cancer cells, including a detailed study of the mechanism of action of the agent. In the future, confirmation of the prominent metabolic pathways deduced from metabolomics should be achieved by enzyme tests, reverse transcriptomics, or genomics (11). Our results were consistent with metabolomic and reverse transcriptomic analyses, and show that metabolomics can serve as an important tool in cancer research.

Acknowledgements

This study was partly supported by Grants-in-Aid for Scientific Research (KAKENHI) (nos. 18659405 and 19591627) from the Ministry of Education, Culture, Sports, Science and Technology, Japan, and by Tsuchiya Foundation Scholarship and Takeda Science Foundation Scholarship. This work was carried out at the Analysis Center of Life Science, Natural Science Center for Basic Research and Development, Hiroshima University.

References

1. Jemal A, Siegel R, Ward E, *et al*: Cancer statistics, 2006. CA Cancer J Clin 56: 106-130, 2006.
2. Koizumi W, Narahara H, Hara T, *et al*: S-1 plus cisplatin versus S-1 alone for first-line treatment of advanced gastric cancer (SPIRITS trial): a phase III trial. Lancet Oncol 9: 215-221, 2008.
3. Cunningham D, Starling N, Rao S, *et al*: Capecitabine and oxaliplatin for advanced esophagogastric cancer. N Eng J Med 358: 36-46, 2008.
4. Van Cutsem E, Moiseyenko VM, Tjulandin S, *et al*: Phase III study of docetaxel and cisplatin plus fluorouracil compared with cisplatin and fluorouracil as first-line therapy for advanced gastric cancer: a report of the V325 Study Group. J Clin Oncol 24: 4991-4997, 2006.
5. Sumner LW, Mendes P and Dixon RA: Plant metabolomics: large-scale phytochemistry in the functional genomics era. Phytochemistry 62: 817-836, 2003.
6. Schauer N, Semel Y, Roessner U, *et al*: Comprehensive metabolic profiling and phenotyping of interspecific introgression lines for tomato improvement. Nat Biotechnol 24: 447-454, 2006.
7. Plumb R, Granger J, Stumpf C, Wilson ID, Evans JA and Lenz EM: Metabonomic analysis of mouse urine by liquid-chromatography-time of flight mass spectrometry (LC-TOFMS): detection of strain, diurnal and gender differences. Analyst 128: 819-823, 2003.
8. Opstad KS, Bell BA, Griffiths JR and Howe FA: An assessment of the effects of sample ischaemia and spinning time on the metabolic profile of brain tumour biopsy specimens as determined by high-resolution magic angle spinning (1)H NMR. NMR Biomed 21: 1138-1147, 2008.
9. Bayet-Robert M, Loiseau D, Rio P, *et al*: Quantitative two-dimentional HRMAS ^{1}H-NMR spectroscopy-based metabolite profiling of human cancer cell lines and response to chemotherapy. Magn Reson Med 63: 1172-1183, 2010.
10. Bayet-Robert M, Lim S, Barthomeuf C and Morvan D: Biochemical disorders induced by cytotoxic marine natural products in breast cancer cells as revealed by proton NMR spectroscopy-based metabolomics. Biochem Pharmacol 80: 1170-1179, 2010.
11. Morvan D and Demidem A: Metabolomics by proton nuclear magnetic resonance spectroscopy of the response to chloroethylnitrosourea reveals drug efficacy and tumor adaptive metabolic pathways. Cancer Res 67: 2150-2159, 2007.
12. Tsutani Y, Yoshida K, Sanada Y, *et al*: Decreased orotate phosphoribosyltransferase activity produces 5-fluorouracil resistance in a human gastric cancer cell line. Oncol Rep 99: 2268-2273, 2008.
13. Hirayama A, Kami K, Sugimoto M, *et al*: Quantitative metabolome profiling of colon and stomach cancer microenvironment by capillary electrophoresis time-of-flight mass spectrometry. Cancer Res 69: 4918-4925, 2009.
14. Chen JL, Tang HQ, Hu JD, *et al*: Metabolomics of gastric cancer metastasis detected by gas chromatography and mass spectrometry. World J Gastroenterol 16: 5874-5880, 2010.
15. Mohamed R, Varesio E, Ivosev G, *et al*: Comprehensive analytical strategy for biomarker identification based on liquid chromatography coupled to mass spectrometry and new candidate confirmation tools. Anal Chem 81: 7677-7694, 2009.
16. Ogata H, Goto S, Sato K, Fujibuchi W, Bono H and Kanehisa M: KEGG: Kyoto encyclopedia of genes and genomics. Nucleic Acids Res 27: 29-34, 1999.
17. Horai H, Arita M, Kanaya S, *et al*: MassBank: A public repository for sharing mass spectral data for life sciences. J Mass Spectrom 45: 703-714, 2010.
18. Griffin JL and Shockcor JP: Metabolic profiles of cancer cells. Nat Rev Cancer 4: 551-561, 2004.
19. Dang CV and Semenza GL: Oncogenic alterations of metabolism. Trends Biochem Sci 24: 68-72, 1999.
20. Fox CJ, Hammerman PS and Thompson CB: Fuel feeds function: energy metabolism and the T-cell response. Nut Rev Immunol 5: 844-852, 2005.
21. Phang JM, Liu W and Zabirnyk O: Proline metabolism and microenvironmental stress. Annu Rev Nutr 30: 441-463, 2010.
22. Cascino A, Muscaritoli M, Cangiano C, *et al*: Plasma amino acid imbalance in patients with lung and breast cancer. Anticancer Res 15: 507-510, 2005.
23. Phang JM: The regulatory functions of proline and pyrroline-5-carboxylic acid. Curr Top Cell Regul 25: 91-132, 1985.
24. White TA, Krishnan N, Becker DF and Tanner JJ: Structure and kinetics of monofunctional proline dehydrogenase from *Thermus thermophilius*. J Biol Chem 282: 14316-14327, 2007.
25. Liu Y, Borchert GL, Surazynski A and Phang JM: Proline oxidase, a p53-induced gene, targets COX-2/PDE2 signaling to induce apoptosis and inhibit tumor growth in colorectal cancers. Oncogene 27: 6729-6737, 2008.
26. Pandhare J, Cooper SK and Phang JM: Proline oxidase, a proapoptotic gene, is induced by triglitazone: evidence for both peroxisomal proliferator-activated receptor gamma-dependent and -independent mechanisms. J Biol Chem 281: 2044-2052, 2006.
27. Liu Y, Borchert GL, Donald SP, Diwan BA, Anver M and Phang JM: Proline oxidase functions as a mitochondrial tumor suppressor in human cancers. Cancer Res 69: 6414-6422, 2009.

Contents lists available at SciVerse ScienceDirect

Pathology – Research and Practice

journal homepage: www.elsevier.com/locate/prp

Original article

Cathepsin D as a potential prognostic marker for lung adenocarcinoma

Takahiro Mimae[a,b,c], Koji Tsuta[a,*], Akiko M. Maeshima[a], Morihito Okada[c], Hisao Asamura[d], Tadashi Kondo[b], Hitoshi Tsuda[a]

[a] Pathology and Clinical Laboratory Division, National Cancer Center Hospital, Tokyo, Japan
[b] Division of Pharmacoproteomics, National Cancer Center Research Institute, Tokyo, Japan
[c] Department of Surgical Oncology, Research Institute for Radiation Biology and Medicine, Graduate School of Biomedical Sciences, Hiroshima University, Hiroshima, Japan
[d] Division of Thoracic Surgery, National Cancer Center Hospital, Tokyo, Japan

ARTICLE INFO

Article history:
Received 13 January 2012
Received in revised form 18 March 2012
Accepted 29 May 2012

Keywords:
Cathepsin D
Lung adenocarcinoma
Tumor marker
Predictive factor
Differentiation

ABSTRACT

We previously identified cathepsin D as a possible marker for lung adenocarcinoma (AD). The purpose of the present study is to evaluate the correlation between cathepsin D expression and clinicopathological findings or prognosis. We conducted immunohistochemistry (IHC) to assess 150 AD tissues. For these 150 tumors, TTF-1 expression, *EGFR* and *KRAS* gene mutations, and *ALK* rearrangements had already been examined. Cathepsin D expression was detected in 44% (66 of 150, IHC score ≥1+) and 27.3% (41 of 150, IHC score ≥2+). Cathepsin D-positive (IHC score ≥2+) tumors were more poorly differentiated than cathepsin D-negative ones, while all lepidic predominant invasive adenocarcinomas showed no cathepsin D expression. Univariate analysis revealed a poor prognosis for cathepsin D-positive lung AD patients with an IHC score ≥2+ ($P = 0.044$). Cathepsin D expression was more frequent in TTF-1-negative than in TTF-1-positive ADs ($P = 0.034$), and more frequent in ADs with *EGFR* wild genotype than mutant *EGFR* ($P < 0.001$). Regarding AD patients with *ALK* rearrangements, 4 were positive for Cathepsin D, while 2 were negative. Cathepsin D expression is indicated to be a possible prognostic marker for lung AD and to correlate with a more poorly differentiated form.

Introduction

The molecular and histopathological features of lung cancer are important for understanding its potential for malignancy and sensitivity to therapies. Lung cancer comprises different subtypes with divergent and heterologous phenotypes; however, as yet, there is no accepted classification system for differentiating tumors on the basis of specific features. In working toward addressing this issue, a newly revised TNM Classification for Lung Cancer was published in 2009 [1]. This classification includes widely validated changes for the staging system [2]. Non-small-cell lung cancer (NSCLC) comprises about 80% of all lung cancers. Lung adenocarcinoma (AD) is the most common histologic subtype of lung cancer in most countries, accounting for almost half of all lung cancers [3]. TNM classification is an important prognostic factor for NSCLCs, including AD, and most patients with pathological (p) Stage I (pStage I) lung AD have a good prognosis. However, 20–30% of patients with pStage I lung AD do have a poor prognosis, and surgical therapy alone is an inadequate form of treatment for them [4]. The TNM classification thus cannot differentiate between these patients with pStage I lung AD, and a new predictive marker is needed to determine whether adjuvant therapy should be performed.

In a previous study, we reported that cathepsin D is expressed at a significantly higher level in lung AD compared with malignant pleural mesothelioma [5]. Cathepsin D is synthesized as a preproenzyme [6] and subsequently forms the intermediate active enzyme (48 kDa) by post-translational modifications. This molecule is divided into the 2-chain (34 and 14 kDa) mature enzyme after further cleavage occurs in the acidic lysosome [7,8]. Under normal conditions, less than 10% of cathepsin D escapes processing and is secreted [9]; however, cathepsin D is secreted aberrantly and excessively in various types of cancers [10,11], and is associated with increased cancer growth, invasion, and metastasis. Thus, this molecule might also be involved in lung AD progression, and may therefore be a useful prognostic marker for this form of cancer. Although previous reports have examined the correlation between cathepsin D expression and prognosis of patients with NSCLC by immunohistochemistry (IHC) [12,13], it is still controversial as to whether cathepsin D has any value as a prognostic indicator.

In the present study, we used IHC to evaluate cathepsin D expression in samples of tumor from patients with lung AD. We

* Corresponding author at: Division of Pathology, National Cancer Center Hospital, 1-1 Tsukiji 5-chome, Chuo-ku, Tokyo 104-0045, Japan. Tel.: +81 3 3542 2511; fax: +81 3 3545 3567.
E-mail address: ktsuta@ncc.go.jp (K. Tsuta).

0344-0338/$ – see front matter © 2012 Elsevier GmbH. All rights reserved.
http://dx.doi.org/10.1016/j.prp.2012.05.020

also analyzed the correlation between cathepsin D expression and clinical features in order to determine the appropriate criteria for evaluating cathepsin D expression. Additionally, we assessed the correlation of cathepsin D expression with thyroid transcription factor 1 (TTF-1) (a marker of lung AD) expression, epidermal growth factor receptor (*EGFR*) and *KRAS* mutation status and anaplastic lymphoma kinase (*ALK*) rearrangements involved in lung AD progression. These data will serve as background information for studies assessing the predictive value of molecular markers for sensitivity to cathepsin D-targeted therapy.

Materials and methods

Patient population

This study included 150 patients with lung invasive AD having undergone surgical resection at the National Cancer Center Hospital (Tokyo, Japan) between 1997 and 2003. An institutional review board approved this study.

All hematoxylin and eosin-stained or Elastica van Gieson stained slides and the immunohistochemical analyses available were reviewed by pathologists (T.M. and K.T.). Histologic diagnosis was based on the classification schema of the latest edition of the World Health Organization Classification [14], with the aid of immunohistochemical panels [15]. Furthermore, AD cases were graded on the basis of differentiation in a 3-tiered system. Briefly, well-differentiated tumors were consistent with predominant lepidic or papillary patterns, moderately differentiated tumors were consistent with a predominant acinar pattern, and poorly differentiated tumors were consistent with a solid growth pattern [16]. In addition, AD cases were classified according to International Association for the Study of Lung Cancer/American Thoracic Society/European Respiratory Society (IASLC/ATS/ERS) Classification of Lung Adenocarcinoma in Resection Specimens [17].

Tissue microarray construction

The most representative tumor areas were sampled for the tissue microarray (TMA). The TMAs were assembled with a tissue-array instrument (Azumaya, Tokyo, Japan). To reduce sampling bias due to tumor heterogeneity, we used 2 replicate 2.0-mm diameter cores from different areas of individual tumors.

Immunohistochemical analysis

For immunohistochemical staining, 4-μm-thick sections were routinely deparaffinized. The sections were exposed to 3% hydrogen peroxide for 15 min to block endogenous peroxidase activity, and then washed in deionized water for 2–3 min. Heat-induced epitope retrieval was performed with citrate buffer solution (pH 6.0) (Muto Pure Chemicals Co., Japan). After the slides were allowed to cool at room temperature for about 30 min, they were rinsed with deionized water. The slides were then incubated with primary antibodies against cathepsin D (1:1000, 49/cathepsin D; Becton Dickinson, San Jose, CA) and TTF-1 (1:100, 8G7G3/1, Dako) for 1 h at room temperature. Immunoreactions were detected using the Envision-Plus system (Dako), and visualized with 3,3′-diaminobenzidine. Counterstaining was performed with hematoxylin.

IHC scoring system

We evaluated the immunostaining for cathepsin D at magnifications of 40× and 100×, using an Olympus BX40 microscope (Olympus, Tokyo, Japan). Immunoreactivity was classified on the basis of cytoplasmic staining intensity, and the following scoring system was used: negative (Score 0); weak intensity (Score 1), defined as positive immunoreactivity that was only detected at 100× magnification; moderate intensity (Score 2), defined as positive immunoreactivity that was easily detected at 40× magnification, but was weaker than that of intra-alveolar macrophages used as an internal positive control; strong intensity (Score 3), defined as positive immunoreactivity equal to, or more intense, than that of intra-alveolar macrophages. Immunoreactivity was defined as positive if ≥10% of tumor cells stained immunohistochemically positive for each score.

EGFR, KRAS mutational status, and ALK rearrangements

We detected 2 common *EGFR* mutations (deletions in exon 19 [DEL], and a point mutation at codon 858 in exon 21 [L858R]), as well as *KRAS* mutations (exons 1 and 2), using high-resolution melting analysis routinely performed at our institution [18]. *ALK* rearrangements were analyzed by immunohistochemistry, reverse transcription polymerase chain reaction, and/or chromogenic in situ hybridization assay [19].

Statistical analysis

A *t*-test for continuous variables and χ^2 tests for categorical variables were used. A *P* value of ≤0.05 was regarded as significant. Overall survival (OS) curves were calculated using the Kaplan–Meier method. Univariate survival analysis was performed with the log-rank test and Cox proportional hazard regression. The multivariate Cox model was subsequently used to evaluate variables with $P < 0.10$ as indicated by Wald's test. Statistical significance was set at $P \leq 0.05$.

Results

Cathepsin D expression status and clinicopathological findings in patients with lung AD

Representative cases of positive cathepsin D expression detected using IHC for lung AD are shown in Fig. 1a–c while negative cathepsin D expression for normal lung alveolar cells is shown in Fig. 1d. We evaluated all 150 cases of lung AD for cathepsin D immunoreactivity, using 2 criteria, namely, an IHC score ≥1+ or ≥2+. The cathepsin D expression rate for an IHC score of ≥1+ was 44% (66 of 150 cases), while the rate for a score of ≥2+ was 27.3% (41 of 150 cases).

The study cohort included 89 male and 61 female patients. The mean age at the time of diagnosis was 63.1 years (range, 37–82 years), and 84 of the patients were smokers. Lung AD tumors were grouped according to their histomorphology: 49 tumors were well differentiated, 52 were moderately differentiated, and 49 were poorly differentiated. With regard to the p-stage, 82 patients had lymph node metastasis while 100 patients had pStage I or II tumors (TNM 7th edition). Tumor size ranged from 1.1 to 9.0 cm (mean, 3.23 cm) (Table 1). The median follow-up time was 94.1 months (range, 2.3–146.9 months). The 5-year survival rate in this patient cohort was 63.1% (95% confidence interval, 59.2–67.1%), with 82 patients still alive at the time of this report.

We adopted the criterion of IHC score ≥2+ as indicative of positive cathepsin D expression, because cathepsin D expression and OS were only significantly correlated at this IHC score ($P = 0.044$). No significant differences were detected between cathepsin D expression and sex, age, smoking, lymph node metastasis, tumor stage, or tumor size (Table 1). Cathepsin D positive immunostaining was more frequently observed in poorly than in well-differentiated cases of AD ($P < 0.001$); poorly differentiated AD was significantly correlated with cathepsin D expression, compared to moderately

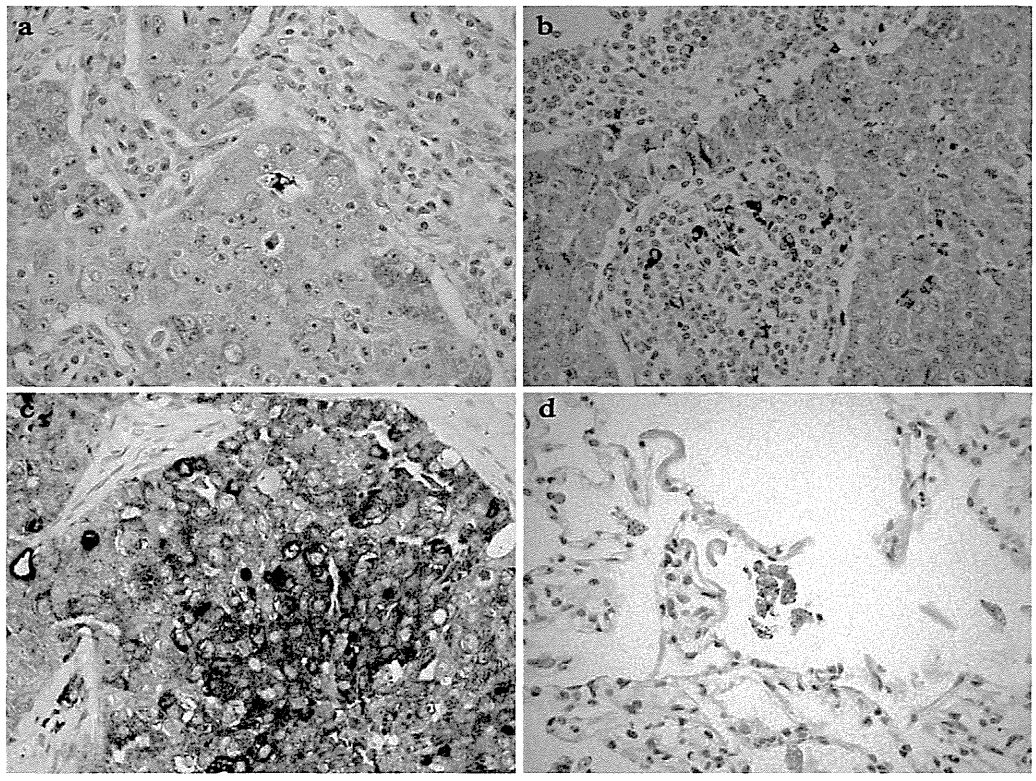

Fig. 1. Cathepsin D immunohistochemical scoring in lung AD. (a) Weak intensity (score 1), (b) moderate intensity (score 2), and (c) strong intensity (score 3) are shown (40×). (d) Negative intensity is detected in normal lung alveolar cells, whereas macrophage cells show positive intensity (40×).

differentiated AD ($P=0.007$) (Table 1). According to histological subtypes, cathepsin D expression frequency became high in the order of lepidic, acinar, papillary, micropapillary, and solid predominant with mucin production. Cathepsin D expression was frequently detected in solid or papillary compared to lepidic predominant with statistical significance ($P<0.001$ or $P=0.009$). No cathepsin D expression was observed in lepidic predominant invasive adenocarcinoma (Table 1).

Correlation of OS with clinicopathologic factors and cathepsin D expression status

We investigated the correlation of the patients' OS and clinicopathologic factors with cathepsin D expression. The 5-year OS rates for patients with cathepsin D-positive and negative AD (using the IHC score ≥2+ criterion) were 58.5% and 64.8%, respectively ($P=0.044$); however, using the IHC score ≥1+ criterion, the 5-year OS rates with cathepsin D-positive and cathepsin D-negative AD were 63.9% and 63.6%, respectively ($P=0.49$) (Fig. 2 and Table 2).

Multivariate analysis revealed that older age ($P=0.009$), poor tumor differentiation ($P=0.029$), and larger tumor size ($P=0.039$) were significantly correlated with a poor prognosis. However, no significant correlation was detected between cathepsin D expression and the 5-year OS ($P=0.53$) (Table 2).

Cathepsin D and TTF-1 expression, EGFR and KRAS mutations, and ALK rearrangements

A significant difference was detected in the co-expression status of cathepsin D and TTF-1 ($P=0.034$) (Table 3): 39.5% (17 of 43 cases) of patients had lung AD that was negative for TTF-1, but positive for cathepsin D.

To further characterize cathepsin D-positive lung AD, we assessed the correlation between cathepsin D expression status

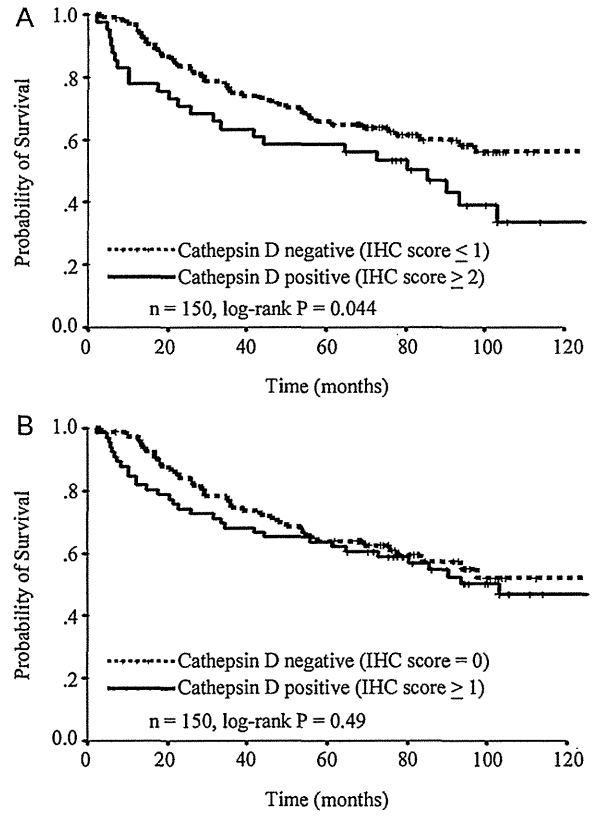

Fig. 2. OS curves are shown for the patients with each cathepsin IHC score. (a) OS according to cathepsin D IHC score (positive, IHC score ≥2; negative, IHC score ≤1). (b) OS according to cathepsin D IHC score (positive, IHC score ≥1; negative, IHC score = 0).

Table 1
Patient characteristics according to cathepsin D IHC[a] score.

Variable	All Patients	IHC score ≥2+			P
		Positive	Negative		
Sex					
Male	89	29	60		0.081
Female	61	12	49		
Age					
Mean	63.1	63.6	62.9		0.68
Range	37–82	41–82	37–82		
Smoking					
Non-smoker	66	17	49		0.70
Smoker	84	24	60		
Differentiation					
Well	49	5	44	w[b] vs. m[c]	0.084
Moderate	52	12	40	w vs. p[d]	<0.001
Poor	49	24	25	m vs. p	0.007
Histological subtype[e]					
Lepidic predominant	31	0	31		<0.001
Acinar predominant	20	5	15		
Papillary predominant	43	10	33		
Micropapillary predominant	7	2	5		
Solid predominant with mucin production	49	24	25		
pT factor					
pT1a+1b+2a+2b	117	29	88		0.19
pT3+4	33	12	21		
Lymph node metastasis					
Negative	84	21	63		0.45
Positive	62	19	43		
pStage[f] (TNM)					
I + II	103	27	76		0.62
III + IV	43	13	30		
Tumor size (cm)					
Mean	3.23	3.68	3.15		0.11
Range	1.1–9.0	1.2–9.0	1.1–7.5		

[a] Immunohistochemistry.
[b] Well differentiation.
[c] Moderate differentiation.
[d] Poor differentiation.
[e] According to International Association for the Study of Lung Cancer/American Thoracic Society/European Respiratory Society Classification of Lung Adenocarcinoma in Resection Specimens.
[f] Pathological stage.

Table 2
Univariate and multivariate analysis for overall survival.

Variable	Univariate analysis			Final multivariate analysis		
	HR[a]	95% CI[b]	P	HR	95% CI	P
Sex						
Female vs. male	0.84	0.52–1.36	0.48			
Age						
<70 vs. ≥70	2.17	1.32–3.57	0.002	2.05	1.20–3.51	0.009
Smoking						
Non-smoker vs. smoker	0.86	0.54–1.39	0.54			
Differentiation						
Well vs. moderate + poor	4.56	2.26–9.21	<0.001	2.41	1.10–5.28	0.029
pT factor						
pT1a+1b+2a+2b vs. pT3+4	2.07	1.24–3.47	0.006	1.10	0.59–2.06	0.76
Lymph node metastasis						
Negative vs. positive	3.31	2.00–5.47	<0.001	1.71	0.81–3.62	0.16
pStage[c] (TNM)						
I + II vs. III + IV	2.96	1.81–4.84	<0.001	1.53	0.73–3.22	0.26
Tumor size (cm)						
<3.0 vs. ≥3.0	2.29	1.41–3.72	0.001	1.78	1.03–3.08	0.039
Cathepsin D IHC[d] score ≥1+						
Negative vs. positive	1.18	0.73–1.90	0.49	Not analyzed		
Cathepsin D IHC score ≥2+						
Negative vs. positive	1.66	1.01–2.73	0.044	1.18	0.70–2.01	0.53

[a] Hazard ratio (the later group to the former group).
[b] Confidence interval.
[c] Pathological stage.
[d] Immunohistochemistry.

Table 3
Patient characteristics according to cathepsin D and TTF-1[a] IHC[b] score and EGFR[c], KRAS, and ALK[d] mutation.

Variable	All patients	TTF-1		P	EGFR mutation		P	KRAS mutation		P	ALK mutation		P
		Positive	Negative		Positive	Negative		Positive	Negative		Positive	Negative	
Cathepsin D													
Positive	41	24	17	0.034	7	34	<0.001	6	35	0.83	4	37	0.027
Negative	109	83	26		58	50		17	89		2	107	

[a] Thyroid transcription factor 1.
[b] Immunohistochemistry.
[c] Epidermal growth factor receptor.
[d] Anaplastic lymphoma kinase.

and *EGFR* and *KRAS* mutations, or *ALK* rearrangements. Most of the patients with cathepsin D expression showed an *EGFR* wild genotype ($P < 0.001$). There was no statistical difference in the *KRAS* mutation rate between patients who were positive for cathepsin D and those who were not ($P = 0.83$). Among the patients with lung AD with *ALK* rearrangements, 4 were positive for cathepsin D, while 2 were negative. *ALK* rearrangements were frequently detected in cathepsin D-positive lung AD compared to cathepsin D-negative lung AD ($P = 0.027$) (Table 3).

Discussion

In this study, we demonstrated that cathepsin D is a prognostic marker for lung AD. To our knowledge, this study is also the first to report a poor prognosis in patients with cathepsin D-positive lung AD. Poorly or moderately differentiated adenocarcinoma and solid predominant with mucin production invasive adenocarcinoma had a high frequency of cathepsin D expression compared to others. In addition, we have established possible criteria for immunohistochemical evaluation of cathepsin D expression in lung AD.

Tumor expression of cathepsin D is considered to be a poor prognostic factor. There is increasing evidence in several studies that cathepsin D expression is significantly related to cancer progression [10,20–26]. In the present study, univariate analysis revealed that cathepsin D expression by tumor cells correlated with an adverse prognosis in patients with lung AD. A previous study, however, reported a good prognosis in patients with cathepsin D-positive NSCLC [13]. Another report showed an unfavorable prognosis for patients with lung AD positive for cathepsin D expression in stromal cells around the tumor cells, but not in the actual tumor cells [12]. One possible reason for these contrasting results is that the previous reports included not only AD, but also other types of NSCLC. This present study suggests that cathepsin D is involved in malignant progression of lung AD, but it remains unclear as to whether this is the case for other types of NSCLC. Immunohistochemical expression of cathepsin D has also frequently been observed in cases of advanced stage adenocarcinoma of the breast [27,28]. The findings also supported the result of this study.

On the other hand, no significant correlation was found between cathepsin D expression and OS by multivariate analysis. One possible reason for these observations is that tumor differentiation confounded the analysis for cathepsin D status. In this study, cases of cathepsin D-positive lung AD showed poorer tumor cell differentiation. In addition, more than a half of cathepsin D-positive lung AD showed the solid predominant subtype, whose differentiation is poorer than other subtypes, and none of them showed the lepidic predominant subtype, which is the most well-differentiated subtype among invasive adenocarcinomas. Univariate and multivariate analyses revealed that patients with moderately or poorly differentiated lung AD had a poorer prognosis compared to those with well-differentiated AD. For each tumor differentiation group, cathepsin D expression did not significantly correlate with prognosis (data not shown). Although it is controversial whether tumor differentiation has any significant correlation with prognosis [17], previous reports have also shown an unfavorable prognosis in patients with poorly differentiated lung AD [29–31]. Other clinical variables did not confound the multivariate analysis results, because they were not significantly correlated with cathepsin D expression.

We also found cathepsin D to be a possible predictive marker for lung AD with *ALK* rearrangements. *ALK* rearrangements have been frequently detected in patients with moderately to poorly differentiated AD, while the EGFR mutation was found in patients with well- to moderately differentiated AD [32,33]. A previous study showed that lung AD patients with *ALK* rearrangements, or the *EGFR* wild genotype, had a poor prognosis [33–36]. In addition, one study detected *ALK* rearrangements in more than half of the patients with lung AD exhibiting histologic features (solid or acinar growth pattern, cribriform structure, or the presence of signet-ring cells) that correspond to moderately or poorly differentiated tumors [37].

Recent clinical trials have revealed that accurate histologic typing of NSCLC, especially with regard to diagnosis of squamous cell carcinoma (SCC), is essential [38,39]. Differentiation of lung AD from SCC is therefore a key aspect of histologic typing because both are major histological types of NSCLC. TTF-1 is derived from peripheral alveolar cells and is used as a marker for primary lung AD. Previous reports have shown TTF-1 expression to be detected in 45–83% of lung AD cases [40–43]; however, in about 30% of patients with lung AD, TTF-1 expression was negative. In the present study, cathepsin D was found to be a useful immunohistochemical marker for the diagnosis of lung AD, because about 40% of TTF-1 negative patients were positive for cathepsin D. In addition, a previous report showed that lungs affected by SCC had a significantly lower level of cytosolic cathepsin D compared to the normal lung, using an immunoradiometric assay [44]. Thus, cathepsin D is a useful marker for the diagnosis of lung AD, and may also help to distinguish AD from SCC of the lung.

Whether cathepsin D represents a target for tumor therapy is controversial; however, *in vivo* and *in vitro* studies have demonstrated that cathepsin D exerts stimulatory effects on breast cancer progression [22,24,26]. Many lysosomal enzymes, including cathepsin D, are over-expressed in cancer cells [45,46], and tumor cell death in some of these cases might be caspase-independent, without involving the classic caspase-dependent pathways of apoptosis. Thus, induction of lysosomal cell death pathways represents a possible therapeutic strategy in various cancers [47]. With regard to lysosomal membrane destabilization, 2 methods have therapeutic potentials: (1) formation of reactive oxygen species by irradiation or by enzymatic activities, and (2) lysosomal membrane permeabilization by lysosomotropic compounds. Irradiation is commonly used clinically for cancer therapy, and the use of lysosomotropic compounds to sensitize tumor cells to anticancer drugs may also represent a new therapeutic possibility [48]. Although the exact relationship between cathepsin D expression and tumor progression in lung AD remains unclear, we think that this molecule is a potential target in the treatment of cathepsin D-positive lung AD.

In summary, we found that Cathepsin D expression is a potential marker for lung AD. Furthermore, most cases of Cathepsin D-positive lung AD were moderately or poorly differentiated, and patients with these types of AD may have a poor prognosis. Prospective studies involving more numbers of cases are necessary to further validate these associations.

Conflict of interest

The authors declare that they have no conflict of interest.

Acknowledgments

This work was supported in part by a Grant-in-Aid for Cancer Research from the Ministry of Health, Labor and Welfare of Japan (H.T.). We would like to thank Ms. Sachiko Miura and Ms. Chizu Kina for their skillful technical assistance.

References

[1] F.C. Detterbeck, D.J. Boffa, L.T. Tanoue, The new lung cancer staging system, Chest 136 (2009) 260–271.
[2] P.A. Groome, V. Bolejack, J.J. Crowley, C. Kennedy, M. Krasnik, L.H. Sobin, P. Goldstraw, The IASLC Lung Cancer Staging Project: validation of the proposals for revision of the T N, and M descriptors and consequent stage groupings in the forthcoming (seventh) edition of the TNM classification of malignant tumours, J. Thorac. Oncol. 2 (2007) 694–705.
[3] S.S. Devesa, F. Bray, A.P. Vizcaino, D.M. Parkin, International lung cancer trends by histologic type: male:female differences diminishing and adenocarcinoma rates rising, Int. J. Cancer 117 (2005) 294–299.
[4] A.G. Little, T.R. DeMeester, M.K. Ferguson, D.B. Skinner, P.C. Hoffman, C. Skosey, R.R. Blough, H.M. Golomb, Modified stage I (T1N0M0 T2N0M0), nonsmall cell lung cancer: treatment results, recurrence patterns, and adjuvant immunotherapy, Surgery 100 (1986) 621–628.
[5] M. Hosako, T. Muto, Y. Nakamura, K. Tsuta, N. Tochigi, H. Tsuda, H. Asamura, T. Tomonaga, A. Kawai, T. Kondo, Proteomic study of malignant pleural mesothelioma by laser microdissection and two-dimensional difference gel electrophoresis identified cathepsin D as a novel candidate for a differential diagnosis biomarker, J. Proteomics 75 (2011) 833–844.
[6] K. von Figura, A. Hasilik, Lysosomal enzymes and their receptors, Annu. Rev. Biochem. 55 (1986) 167–193.
[7] A. Hasilik, E.F. Neufeld, Biosynthesis of lysósomal enzymes in fibroblasts. Phosphorylation of mannose residues, J. Biol. Chem. 255 (1980) 4946–4950.
[8] S. Kornfeld, I. Mellman, The biogenesis of lysosomes, Annu. Rev. Cell Biol. 5 (1989) 483–525.
[9] F. Dittmer, R. Pohlmann, K. von Figura, The phosphorylation pattern of oligosaccharides in secreted procathepsin D is glycosylation site-specific and independent of the expression of mannose 6-phosphate receptors, J. Biol. Chem. 272 (1997) 852–858.
[10] M. Garcia, D. Derocq, P. Pujol, H. Rochefort, Overexpression of transfected cathepsin D in transformed cells increases their malignant phenotype and metastatic potency, Oncogene 5 (1990) 1809–1814.
[11] H. Rochefort, F. Capony, M. Garcia, V. Cavailles, G. Freiss, M. Chambon, M. Morisset, F. Vignon, Estrogen-induced lysosomal proteases secreted by breast cancer cells: a role in carcinogenesis? J. Cell. Biochem. 35 (1987) 17–29.
[12] M. Higashiyama, O. Doi, K. Kodama, H. Yokouchi, T. Kasugai, S. Ishiguro, Influence of cathepsin D expression in lung adenocarcinoma on prognosis: possible importance of its expression in tumor cells and stromal cells, and its intracellular polarization in tumor cells, J. Surg. Oncol. 65 (1997) 10–19.
[13] Z. Wang, X. Zhao, Expression and prognostic relation of cathepsin D in non-small cell lung cancer tissues and lymph nodes, Zhonghua Jie He He Hu Xi Za Zhi 21 (1998) 164–166.
[14] W.D. Travis, E. Brambilla, H.K. Muller-Hermelink, C.C. Harris, Pathology and genetics tumors of the lung, pleura, thymus and heart, in: World Health Organization Classification of Tumours, IARC Press, Lyon, 2004.
[15] K. Tsuta, Y. Tanabe, A. Yoshida, F. Takahashi, A.M. Maeshima, H. Asamura, H. Tsuda, Utility of 10 immunohistochemical markers including novel markers (desmocollin-3, glypican 3 S100A2, S100A7, and Sox-2) for differential diagnosis of squamous cell carcinoma from adenocarcinoma of the Lung, J. Thorac. Oncol. 6 (2011) 1190–1199.
[16] J.L.C. Society, General Rule for Clinical and Pathologic Recording of Lung Cancer, 5th ed., Kanahara, Tokyo, 1999.
[17] W.D. Travis, E. Brambilla, M. Noguchi, A.G. Nicholson, K.R. Geisinger, Y. Yatabe, D.G. Beer, C.A. Powell, G.J. Riely, P.E. Van Schil, K. Garg, J.H. Austin, H. Asamura, V.W. Rusch, F.R. Hirsch, G. Scagliotti, T. Mitsudomi, R.M. Huber, Y. Ishikawa, J. Jett, M. Sanchez-Cespedes, J.P. Sculier, T. Takahashi, M. Tsuboi, J. Vansteenkiste, I. Wistuba, P.C. Yang, D. Aberle, C. Brambilla, D. Flieder, W. Franklin, A. Gazdar, M. Gould, P. Hasleton, D. Henderson, B. Johnson, D. Johnson, K. Kerr, K. Kuriyama, J.S. Lee, V.A. Miller, I. Petersen, V. Roggli, R. Rosell, N. Saijo, E. Thunnissen, M. Tsao, D. Yankelewitz, International association for the study of lung cancer/American thoracic society/European respiratory society international multidisciplinary classification of lung adenocarcinoma, J. Thorac. Oncol. 6 (2011) 244–285.
[18] T. Fukui, Y. Ohe, K. Tsuta, K. Furuta, H. Sakamoto, T. Takano, H. Nokihara, N. Yamamoto, I. Sekine, H. Kunitoh, H. Asamura, T. Tsuchida, M. Kaneko, M. Kusumoto, S. Yamamoto, T. Yoshida, T. Tamura, Prospective study of the accuracy of EGFR mutational analysis by high-resolution melting analysis in small samples obtained from patients with non-small cell lung cancer, Clin. Cancer Res. 14 (2008) 4751–4757.
[19] A. Yoshida, K. Tsuta, H. Nitta, Y. Hatanaka, H. Asamura, I. Sekine, T.M. Grogan, M. Fukayama, T. Shibata, K. Furuta, T. Kohno, H. Tsuda, Bright-field dual-color chromogenic in situ hybridization for diagnosing echinoderm microtubule-associated protein-like 4-anaplastic lymphoma kinase-positive lung adenocarcinomas, J. Thorac. Oncol. 6 (2011) 1677–1686.
[20] G. Berchem, M. Glondu, M. Gleizes, J.P. Brouillet, F. Vignon, M. Garcia, E. Liaudet-Coopman, Cathepsin-D affects multiple tumor progression steps in vivo: proliferation, angiogenesis and apoptosis, Oncogene 21 (2002) 5951–5955.
[21] M. Glondu, P. Coopman, V. Laurent-Matha, M. Garcia, H. Rochefort, E. Liaudet-Coopman, A mutated cathepsin-D devoid of its catalytic activity stimulates the growth of cancer cells, Oncogene 20 (2001) 6920–6929.
[22] M. Glondu, E. Liaudet-Coopman, D. Derocq, N. Platet, H. Rochefort, M. Garcia, Down-regulation of cathepsin-D expression by antisense gene transfer inhibits tumor growth and experimental lung metastasis of human breast cancer cells, Oncogene 21 (2002) 5127–5134.
[23] L. Hu, J.M. Roth, P. Brooks, J. Luty, S. Karpatkin, Thrombin up-regulates cathepsin D which enhances angiogenesis, growth, and metastasis, Cancer Res. 68 (2008) 4666–4673.
[24] Z. Khalkhali-Ellis, D.E. Abbott, C.M. Bailey, W. Goossens, N.V. Margaryan, S.L. Gluck, M. Reuveni, M.J. Hendrix, IFN-gamma regulation of vacuolar pH, cathepsin D processing and autophagy in mammary epithelial cells, J. Cell. Biochem. 105 (2008) 208–218.
[25] E. Liaudet, M. Garcia, H. Rochefort, Cathepsin D, maturation and its stimulatory effect on metastasis are prevented by addition of KDEL retention signal, Oncogene 9 (1994) 1145–1154.
[26] S.S. Ohri, A. Vashishta, M. Proctor, M. Fusek, V. Vetvicka, The propeptide of cathepsin D increases proliferation, invasion and metastasis of breast cancer cells, Int. J. Oncol. 32 (2008) 491–498.
[27] S. Aziz, S. Pervez, S. Khan, N. Kayani, M. Rahbar, Immunohistochemical cathepsin-D expression in breast cancer: correlation with established pathological parameters and survival, Pathol. Res. Pract. 197 (2001) 551–557.
[28] T. Jahkola, T. Toivonen, K. von Smitten, I. Virtanen, V.M. Wasenius, C. Blomqvist, Cathepsin-D, urokinase plasminogen activator and type-1 plasminogen activator inhibitor in early breast cancer: an immunohistochemical study of prognostic value and relations to tenascin-C and other factors, Br. J. Cancer 80 (1999) 167–174.
[29] C.K. Chung, R. Zaino, J.A. Stryker, M. O'Neill Jr., W.E. DeMuth Jr., Carcinoma of the lung: evaluation of histological grade and factors influencing prognosis, Ann. Thorac. Surg. 33 (1982) 599–604.
[30] A. Gajra, N. Newman, G.P. Gamble, N.Z. Abraham, L.J. Kohman, S.L. Graziano, Impact of tumor size on survival in stage IA non-small cell lung cancer: a case for subdividing stage IA disease, Lung Cancer 42 (2003) 51–57.
[31] Y. Ichinose, T. Yano, H. Asoh, H. Yokoyama, I. Yoshino, Y. Katsuda, Prognostic factors obtained by a pathologic examination in completely resected non-small-cell lung cancer. An analysis in each pathologic stage, J. Thorac. Cardiovasc. Surg. 110 (1995) 601–605.
[32] N. Nose, K. Sugio, T. Oyama, T. Nozoe, H. Uramoto, T. Iwata, T. Onitsuka, K. Yasumoto, Association between estrogen receptor-beta expression and epidermal growth factor receptor mutation in the postoperative prognosis of adenocarcinoma of the lung, J. Clin. Oncol. 27 (2009) 411–417.
[33] S.H. Ou, A. Ziogas, J.A. Zell, Primary signet-ring carcinoma (SRC) of the lung: a population-based epidemiologic study of 262 cases with comparison to adenocarcinoma of the lung, J. Thorac. Oncol. 5 (2010) 420–427.
[34] T.Y. Chou, C.H. Chiu, L.H. Li, C.Y. Hsiao, C.Y. Tzen, K.T. Chang, Y.M. Chen, R.P. Perng, S.F. Tsai, C.M. Tsai, Mutation in the tyrosine kinase domain of epidermal growth factor receptor is a predictive and prognostic factor for gefitinib treatment in patients with non-small cell lung cancer, Clin. Cancer Res. 11 (2005) 3750–3757.
[35] H. Haneda, H. Sasaki, N. Lindeman, O. Kawano, K. Endo, E. Suzuki, S. Shimizu, H. Yukiue, Y. Kobayashi, M. Yano, Y. Fujii, A correlation between EGFR gene mutation status and bronchioloalveolar carcinoma features in Japanese patients with adenocarcinoma, Jpn. J. Clin. Oncol. 36 (2006) 69–75.
[36] M. Sonobe, M. Kobayashi, M. Ishikawa, R. Kikuchi, E. Nakayama, T. Takahashi, T. Menju, K. Takenaka, R. Miyahara, C.L. Huang, K. Okubo, T. Bando, H. Date, Impact of KRAS and EGFR gene mutations on recurrence and survival in patients with surgically resected lung adenocarcinomas, Ann. Surg. Oncol., in press.
[37] A. Yoshida, K. Tsuta, H. Nakamura, T. Kohno, F. Takahashi, H. Asamura, I. Sekine, M. Fukayama, T. Shibata, K. Furuta, H. Tsuda, Comprehensive histologic analysis of ALK-rearranged lung carcinomas, Am. J. Surg. Pathol. 35 (2011) 1226–1234.
[38] D.C. Paech, A.R. Weston, N. Pavlakis, A. Gill, N. Rajan, H. Barraclough, B. Fitzgerald, M. Van Kooten, A systematic review of the interobserver variability for histology in the differentiation between squamous and nonsquamous non-small cell lung cancer, J. Thorac. Oncol. 6 (2011) 55–63.
[39] A. Sandler, Bevacizumab in non small cell lung cancer, Clin. Cancer Res. 13 (2007) s4613–s4616.

[40] V.K. Anagnostou, K.N. Syrigos, G. Bepler, R.J. Homer, D.L. Rimm, Thyroid transcription factor 1 is an independent prognostic factor for patients with stage I lung adenocarcinoma, J. Clin. Oncol. 27 (2009) 271–278.
[41] D.M. Lin, S.M. Zou, N. Lu, P. Wen, X.Y. Liu, Z.G. He, TTF-1 expression and its diagnostic application in lung carcinomas, Zhonghua Zhong Liu Za Zhi 26 (2004) 615–617.
[42] S.J. Martins, T.Y. Takagaki, A.G. Silva, C.P. Gallo, F.B. Silva, V.L. Capelozzi, Prognostic relevance of TTF-1 and MMP-9 expression in advanced lung adenocarcinoma, Lung Cancer 64 (2009) 105–109.
[43] Y. Yatabe, T. Mitsudomi, T. Takahashi, TTF-1 expression in pulmonary adenocarcinomas, Am. J. Surg. Pathol. 26 (2002) 767–773.
[44] A. Ruibal, M.I. Nunez, C. Rio Mdel, S. Garcia Diez, J. Rodriguez, J.F. Alvarez de Linera, Cytosolic cathepsin D levels in squamous carcinomas of the lung, Med. Clin. (Barc.) 120 (2003) 81–84.
[45] N.J. Agnantis, A.C. Goussia, A. Batistatou, D. Stefanou, Tumor markers in cancer patients. An update of their prognostic significance. Part II, In Vivo 18 (2004) 481–488.
[46] W.A. Reid, M.J. Valler, J. Kay, Immunolocalization of cathepsin D in normal and neoplastic human tissues, J. Clin. Pathol. 39 (1986) 1323–1330.
[47] M.E. Guicciardi, M. Leist, G.J. Gores, Lysosomes in cell death, Oncogene 23 (2004) 2881–2890.
[48] E. Agostinelli, N. Seiler, Lysosomotropic compounds and spermine enzymatic oxidation products in cancer therapy (review), Int. J. Oncol. 31 (2007) 473–484.

Prognostic significance of using solid versus whole tumor size on high-resolution computed tomography for predicting pathologic malignant grade of tumors in clinical stage IA lung adenocarcinoma: A multicenter study

Yasuhiro Tsutani, MD, PhD,[a] Yoshihiro Miyata, MD, PhD,[a] Haruhiko Nakayama, MD, PhD,[b] Sakae Okumura, MD, PhD,[c] Shuji Adachi, MD, PhD,[d] Masahiro Yoshimura, MD, PhD,[e] and Morihito Okada, MD, PhD[a]

Objectives: The present multicenter study compared the usefulness of the solid tumor size with that of the whole tumor size on preoperative high-resolution computed tomography for predicting pathologic high-grade malignancy (positive lymphatic, vascular, or pleural invasion) and the prognosis of clinical stage IA lung adenocarcinoma.

Methods: We performed high-resolution computed tomography and F-18 fluorodeoxyglucose-positron emission tomography/computed tomography before curative surgical resection in 502 patients with clinical stage IA lung adenocarcinoma. The revised maximum standardized uptake values on F-18 fluorodeoxyglucose-positron emission tomography/computed tomography were used to correct interinstitutional discrepancies. The whole and solid tumor sizes on high-resolution computed tomography were then analyzed in relation to surgical results.

Results: The mean whole and solid tumor size was 1.97 ± 0.59 cm and 1.20 ± 0.88 cm, respectively. The receiver operating characteristics area under the curve for the whole and solid tumor sizes used to identify high-grade malignancy were 0.590 and 0.829, respectively. Multiple logistic regression analyses demonstrated solid tumor size ($P < .001$) and maximum standardized uptake values of the tumor ($P < .001$) as independent variables for the prediction of high-grade malignancy. Multivariate Cox analysis of disease-free survival demonstrated the former (hazard ratio, 2.30; 95% confidence interval, 1.46-3.63; $P < .001$) and latter (hazard ratio, 1.08; 95% confidence interval, 1.00-1.17; $P = .05$) as independent prognostic factors.

Conclusions: The solid tumor size on high-resolution computed tomography and maximum standardized uptake values on positron emission tomography/computed tomography have greater predictive value for high-grade malignancy and prognosis in clinical stage IA lung adenocarcinoma than that of whole tumor size. (J Thorac Cardiovasc Surg 2012;143:607-12)

Recent advances in high-resolution computed tomography (HRCT) and the widespread application of computed tomography (CT) screening have enhanced the discovery of small lung cancers, particularly adenocarcinoma.[1,2] These often contain a nonsolid component that presents as ground glass opacity (GGO) on HRCT.[2,3] Several investigators have reported that GGO is closely associated with bronchioloalveolar carcinoma.[3,4] Noguchi and colleagues[5] reported that type A and B small peripheral adenocarcinomas (localized bronchioloalveolar carcinoma without foci of active fibroblastic proliferation) demonstrated no lymph node metastasis and a favorable prognosis (100% 5-year survival rate). We therefore hypothesized that the GGO component is not related to malignancy and prognosis, implying that only the solid component of the tumor on HRCT (solid tumor size) is indicative of malignancy and prognosis.

The purpose of the present multicenter study was to evaluate and compare the usefulness of the solid tumor size with that of the whole tumor size as seen on preoperative HRCT for determining pathologic high-grade malignancy (positive for lymphatic [LI], vascular [VI], or pleural invasion [PI]) and the prognosis in cases of clinical stage IA lung adenocarcinoma.

PATIENTS AND METHODS

Patients

We enrolled 502 patients with clinical T1N0M0 stage IA lung adenocarcinoma at 4 institutions (Hiroshima University, Kanagawa Cancer Center, Cancer Institute Hospital, and Hyogo Cancer Center) from August 1, 2005

From the Department of Surgical Oncology,[a] Hiroshima University, Hiroshima, Japan; Department of Thoracic Surgery,[b] Kanagawa Cancer Center, Yokohama, Japan; Department of Thoracic Surgery,[c] Cancer Institute Hospital, Tokyo, Japan; and Departments of Radiology[d] and Thoracic Surgery,[e] Hyogo Cancer Center Akashi, Japan.

Disclosures: Authors have nothing to disclose with regard to commercial support.

Received for publication June 30, 2011; revisions received Sept 7, 2011; accepted for publication Oct 20, 2011; available ahead of print Nov 21, 2011.

Address for reprints: Morihito Okada, MD, PhD, Department of Surgical Oncology, Research Institute for Radiation Biology and Medicine, Hiroshima University, 1-2-3 Kasumi, Minami-ku, Hiroshima 734-0037, Japan (E-mail: morihito@hiroshima-u.ac.jp).

0022-5223/$36.00

doi:10.1016/j.jtcvs.2011.10.037

Abbreviations and Acronyms

CI = confidence interval
CT = computed tomography
DFS = disease-free survival
FDG-PET = F-18 fluorodeoxyglucose-positron emission tomography
GGO = ground glass opacity
HR = hazard ratio
HRCT = high-resolution computed tomography
LI = lymphatic invasion
PI = pleural invasion
SUV = standardized uptake value
VI = vascular invasion

to December 31, 2009. HRCT and F-18 fluorodeoxyglucose-positron emission tomography/CT (FDG-PET/CT) followed by curative R0 resection were performed for all patients, who underwent staging according to the 7th edition of the TNM classification of malignant tumors.[6] Sublobar resections (segmentectomy or wedge resection) were allowed if the tumor mainly consisted of GGO or had no lymph node metastasis through intraoperative assessment. The institutional review board of each institution provided appropriate approval for the present multicenter study. They waived the requirement of informed consent from the individual patients for the present retrospective review of the prospective database. The data were compiled in a Microsoft Excel 2010 file (Microsoft, Redmond, WA).

HRCT Scanning

Chest images were obtained using 16-row, multidetector CT, independent of the subsequent FDG-PET/CT examinations. High-resolution images of the tumors were acquired using the following parameters: 120 kVp, 200 mA, 1- to 2-mm section thickness, 512 × 512 pixel resolution, scanning time 0.5 to 1 sec, and a high spatial reconstruction algorithm with a 20-cm field of view and mediastinal (level, 40 HU; width, 400 HU) and lung (level, –600 HU; width, 1600 HU) window settings. GGO was defined as a misty increase in lung attenuation that did not obscure the underlying vascular markings. We defined the solid tumor size as the maximum dimension of the solid component of the lung windows excluding GGO (Figure 1).

FDG-PET/CT Scanning

The patients were instructed to fast for more than 4 hours before intravenous injection of 74 to 370 MBq FDG and then made to relax for at least 1 hour before FDG-PET/CT scanning. Blood glucose was calculated before the tracer injection to confirm a level of less than 150 mg/dL.[7] Patients with blood glucose values of 150 mg/dL or greater were excluded from PET/CT acquisition. The images were obtained using Discovery ST (GE Healthcare, Little Chalfont, UK), Aquiduo (Toshiba Medical Systems, Tochigi, Japan), or Biograph Sensation16 (Siemens Healthcare, Erlangen, Germany) integrated PET/CT scanners. Low-dose, unenhanced CT images of 2- to 4-mm section thickness for attenuation correction and localization of lesions identified by PET were obtained from the head to the pelvic floor of each patient using a standard protocol. Immediately after CT, PET covered the identical axial field of view for 2 to 4 minutes per table position, depending on the condition of the patient and scanner performance. All PET images with a 50-cm field of view were reconstructed using an iterative algorithm with CT-derived attenuation correction. Variations in the standardized uptake values (SUVs) among institutions were minimized using an anthropomorphic body phantom. A calibration factor was analyzed by dividing the actual SUV by the gauged mean SUV in the phantom background to decrease interinstitutional SUV inconsistencies. The final SUV reported in the present study is referred to as the revised maximum SUV (maxSUV).[8,9] The adjustment of the interinstitutional variability in the SUV narrowed the range from 0.89 to 1.24 to 0.97 to 1.18 when the maxSUV ratio was expressed as the maxSUV of each institute relative to the maxSUV of the control institute.

Statistical Analysis

The data are presented as the numbers and percentages or mean ± standard deviation, unless otherwise stated. Pathologic high-grade malignancy was defined as positive LI, VI, or PI. The receiver operating characteristic curves of the whole and solid tumor sizes were used for the prediction of LI, VI, or PI, high-grade malignancy (LI, VI, or PI), and lymph node metastasis. We also performed multiple logistic regression analyses to determine the independent variables related to whole tumor size, solid tumor size, and maxSUV for the prediction of the pathologic finding of high-grade malignancy. Disease-free survival (DFS) was defined as interval from the date of surgery until the first event (relapse or death from any cause) or the last follow-up visit. The duration of DFS was analyzed using the Kaplan-Meier method. Differences in DFS were assessed using the log-rank test. To assess the potential independent effects of clinical tumor size on DFS, we performed multivariate analyses with the Cox proportional hazards model using variables with $P < .05$ on the univariate analyses; $P < .05$ was considered statistically significant. The data were statistically analyzed using the Statistical Package for Social Sciences software, version 10.5 (SPSS, Chicago, Il).

RESULTS

The characteristics of the 502 study patients are summarized in Table 1. The mean follow-up period after surgery was 19.8 ± 12.2 months, during which disease recurred in 29 patients (5.8%). Of the 29 recurrence cases, 9 (1.8%) were local, including mediastinal lymph node metastasis, 3 (0.6%) were local and distant, and 17 (3.4%) were distant. The mean whole tumor and solid tumor size on HRCT was 1.97 ± 0.59 cm and 1.20 ± 0.88 cm, respectively. LI, VI, and PI was evident in 76 (15.1%), 92 (18.3%), and 56 (11.2%) patients, respectively, and the lymph nodes were involved in 38 (7.8%).

The receiver operating characteristic area under the curve values of the whole and solid tumor sizes used for predicting LI, VI, PI, pathologic high-grade malignancy (LI, VI, or PI), and lymph node metastasis are given in Table 2 and Figure 2. The predictability of all outcomes on the basis of solid tumor size was better than that using the whole tumor size for all subjects.

Although a significant relationship was noted between the whole tumor size and maxSUV (decision coefficient, $r^2 = 0.015$; $P = .007$), a much more significant relationship was detected between the solid tumor size and maxSUV ($r^2 = 0.211$, $P < .001$).

The possible predictors of pathologic high-grade malignancy (LI, VI, or PI) were also investigated (Table 3). Although whole tumor size, solid tumor size, and maxSUV were all significant determinants on the univariate analyses, the solid tumor size and maxSUV were significant determinants on multivariate analysis. Whole tumor size was not an independent predictor of high-grade malignancy.

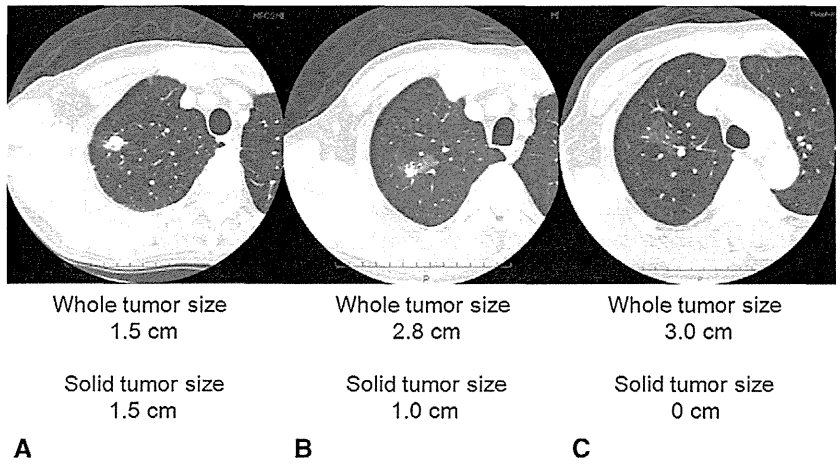

FIGURE 1. Examples of whole and solid tumor sizes on high-resolution computed tomography. A, Whole tumor size, 1.5 cm and solid tumor size, 1.5 cm. B, Whole tumor size, 2.8 cm and solid tumor size, 1.0 cm. C, Whole tumor size, 3.0 cm and solid tumor size, 0 cm.

No significant difference in DFS was identified between patients with a whole tumor size of 2.0 cm or less (n = 289; 3-year DFS rate, 92.5%) and those with a whole tumor size greater than 2.0 cm (n = 213; 3-year DFS rate, 86.7%; $P = .511$; Figure 3, *A*). In contrast, a significant difference in DFS was identified between patients with a solid tumor size of 2.0 cm or less (n = 400; 3-year DFS rate, 93.2%) and those with a solid tumor size greater than 2.0 cm (n = 102; 3-year DFS rate, 78.9%; $P = .013$; Figure 3, *B*).

Univariate analysis of DFS among the 502 patients with adenocarcinoma included preoperative tumor factors (eg, whole tumor size, solid tumor size, and maxSUV; Table 4) as variables. A larger solid tumor size and greater maxSUV were associated with a shorter DFS, but the whole tumor size was not associated with DFS. Moreover, the multivariate analysis that included a solid tumor size and maxSUV as variables demonstrated that solid tumor size (hazard ratio [HR], 2.30; 95% confidence interval [CI], 1.46–3.63; $P < .001$) and maxSUV (HR, 1.08; 95% CI, 1.00–1.17; $P = 0.05$) were independent prognostic factors for DFS (Table 4).

In another multivariate analysis, including the variables of gender, operation type, solid tumor size, maxSUV, and lymph node metastasis, the solid tumor size (HR, 2.00; 95% CI, 1.19–3.36; $P = .009$), maxSUV (HR, 1.10; 95% CI, 1.01–1.20; $P = .034$), and lymph node metastasis (HR, 7.17; 95% CI, 3.18–16.2; $P < .001$) were independent prognostic factors for DFS. In contrast, the whole tumor size was not an independent factor for DFS. However, maxSUV and lymph node metastasis were significant in the model replacing solid tumor size with whole tumor size.

DISCUSSION

The frequency of identification of small lung cancers has increased since CT and enhanced scanning have become routine procedures. Such small tumors, especially in lung adenocarcinomas, often contain GGO components as visualized on HRCT.[1-4,10] Generally, clinical physicians measure the tumor size according to the TNM classification by including the GGO components visualized on HRCT.

On the basis of our hypothesis that the solid components, and not the GGO components, of tumors as visualized on HRCT indicate malignancy and prognosis, we evaluated the role of solid tumor size (the size without the GGO component) in cases of clinical stage IA lung adenocarcinoma

TABLE 1. Patient characteristics

Variable	n = 502
Age (y)	65.3 ± 9.6
Gender	
Male	223 (44.4)
Female	279 (55.6)
Tumor size	
Whole (cm)	1.97 ± 0.59
Solid (cm)	1.20 ± 0.88
MaxSUV	2.84 ± 3.03
Procedure	
Lobectomy	320 (63.7)
Limited (wedge plus segmentectomy)	182 (36.3)
Lymphatic invasion	
Negative	426 (84.9)
Positive	76 (15.1)
Vascular invasion	
Negative	410 (81.7)
Positive	92 (18.3)
Pleural invasion	
Negative	446 (88.8)
Positive	56 (11.2)
Lymph node metastasis	
Negative	464 (92.4)
Positive	38 (7.6)

Data in parentheses are percentages. *maxSUV,* Maximum standardized uptake value.

TABLE 2. Receiver operative characteristic area under the curve values of whole and solid tumor sizes used to predict pathologic findings

	Whole tumor size		Solid tumor size	
Variable	AUC (95% CI)	*P* value	AUC (95% CI)	*P* value
LI	0.560 (0.494–0.626)	.092	0.777 (0.733–0.820)	<.001
VI	0.634 (0.571–0.697)	.001	0.829 (0.789–0.868)	<.001
PI	0.576 (0.499–0.653)	.039	0.771 (0.723–0.820)	<.001
LI or VI or PI	0.590 (0.534–0.646)	.002	0.829 (0.794–0.864)	<.001
N	0.603 (0.519–0.688)	.034	0.761 (0.703–0.819)	<.001

AUC, Area under the curve; *CI,* confidence interval; *LI,* lymphatic invasion; *VI,* vascular invasion; *PI,* pleural invasion; *N,* lymph node metastasis.

and compared its prognostic significance with that of whole tumor size (the size including the GGO component).

All receiver operating characteristic area under the curves for predicting LI, VI, PI, high-grade malignancy, and lymph node metastasis were larger for the solid tumor size than those for the whole tumor size. Moreover, the solid tumor size and maxSUV were identified as independent predictive factors for high-grade malignancy. These findings indicate that the solid tumor size, and not whole tumor size, reflects the pathologic findings related to clinical tumor malignancy. Concerning the relationship between tumor size and lymph node metastasis, we should take account of stage migration because 36% of the patients underwent sublobar resection.

The 7th TNM classification for lung cancer divided the T1 descriptor into T1a (tumors ≤2 cm) and T1b (tumors 2-3 cm) on the basis of the optimal cutoff point for 5-year survival.[11] We analyzed each DFS point in stage IA adenocarcinoma according to the cutoff point of 2 cm using the whole and solid tumor sizes. Although no significant difference in DFS was observed between patients with a whole tumor size of 2.0 cm or less and those with a whole tumor size of greater than 2.0 cm, a significant difference in DFS was identified between patients with a solid tumor

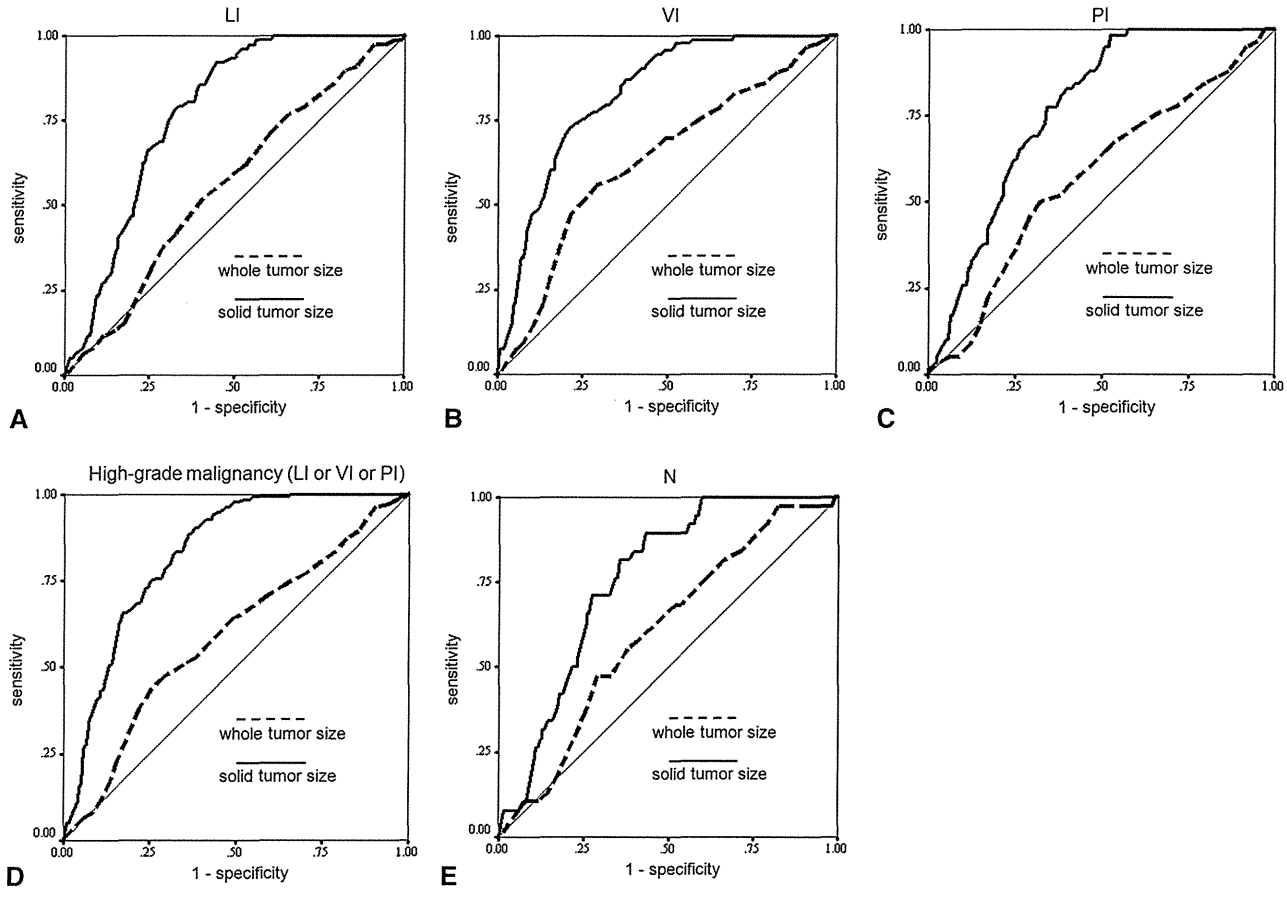

FIGURE 2. Receiver operating characteristic area under the curve for detecting (A) lymphatic invasion *(LI)* (B) vascular invasion *(VI)* (C) pleural invasion *(PI)* (D) high-grade malignancy (LI, VI, or PI), and (E) lymph node metastasis *(N)* for whole and solid tumor sizes.

TABLE 3. Analysis of possible predictors of pathologic high-grade malignancy (positive for lymphatic, vascular, or pleural invasion)

Variable	OR (95% CI)	*P* value
Univariate analysis		
Whole tumor size (cm)	1.70 (1.21–2.39)	.002
Solid tumor size (cm)	4.86 (3.57–6.63)	<.001
MaxSUV	1.51 (1.37–1.66)	<.001
Multivariate analysis		
Model 1		
Whole tumor size (cm)	1.39 (0.94–2.05)	.97
MaxSUV	1.49 (1.35–1.64)	<.001
Model 2		
Solid tumor size (cm)	3.77 (2.69–5.27)	<.001
MaxSUV	1.25 (1.14–1.37)	<.001

OR, Odds ratio; *CI,* confidence interval; *maxSUV,* maximum standardized uptake value.

size of 2.0 cm or less and those with a solid tumor size of greater than 2.0 cm. Furthermore, multivariate Cox analysis revealed that solid tumor size and maxSUV were independent prognostic factors for DFS, and whole tumor size was not. These results have indicated that the solid tumor size more closely correlates with survival and the pathologic findings than does the whole tumor size.

The present study demonstrated that approximately one half of the patients with whole tumors greater than 2 cm could be restaged clinically as having a solid tumor of 2 cm or less. This means that even tumors greater than 2 cm often contain a GGO component. Currently, phase III randomized trials of standard lobectomy versus experimental limited resection for small (≤2 cm in diameter) peripheral nonsmall-cell lung cancers are ongoing in the United States (Cancer and Leukemia Group B trial 14053) and Japan (Japan Clinical Oncology Group trial 0802/West Japan Oncology Group trial 4607L). Among patients with lung adenocarcinomas and a whole tumor size greater than 2.0 cm, 50% have a good prognosis and could be future candidates for limited surgery such as segmentectomy and wedge resection of the lung if the surgical margin is adequate. No difference was seen in DFS among patients with a solid tumor size of 2 cm or less, who were treated with lobectomy versus sublobar resection in the present study (data not shown); however, this finding should be confirmed by prospective studies.

Several investigators have reported that the prognosis of patients with lung adenocarcinoma and a large GGO component visualized on HRCT was much better than that of patients with other adenocarcinoma types, irrespective of the maximal tumor dimension.[12-15] In addition, a large prospective study has examined the specificity, sensitivity, and accuracy of the radiologic diagnoses of lymphatic/vessel invasion and nodal involvement of clinical T1N0M0 adenocarcinoma made according to the HRCT findings.[16] The outcomes failed to corroborate the

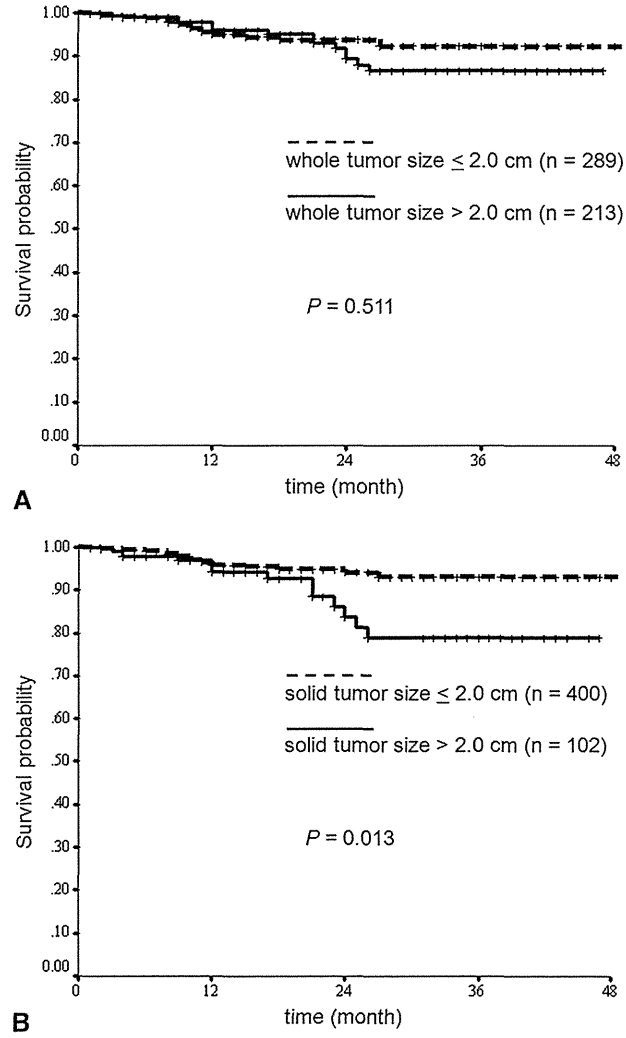

FIGURE 3. Disease-free survival *(DFS)* curves of patients according to tumor size on high-resolution computed tomography. A, Three-year DFS rate of 92.5% and 86.7% for a whole tumor size of 2.0 cm or less and greater than 2.0 cm, respectively ($P = .511$). B, Three-year DFS rate of 93.2% and 78.9% for solid tumor size of less than 2.0 cm and greater than 2.0 cm, respectively ($P = .013$).

predetermined criteria using the GGO ratio for specificity. This indicates that using the solid tumor size is much simpler than using the GGO ratio; furthermore, the solid tumor size can be applied to the T descriptor in the TNM classification.

In the present study, the maxSUV on FDG-PET/CT was also a useful factor for predicting pathologic high-grade malignancy and DFS. We have previously reported on the usefulness of maxSUV on PET/CT as a predictor of malignancy and the prognosis of adenocarcinoma of the lung but not for squamous cell carcinoma of the lung.[8,9,17,18] In those reports, the maxSUV was closely related to the occurrence of LI, VI, PI, and nodal metastasis and was an independent predictive factor for DFS.[8,9,17,18] The interinstitutional

TABLE 4. Univariate and multivariate analyses of disease-free survival

Variable	HR (95% CI)	*P* value
Univariate analysis		
Whole tumor size (cm)	1.47 (0.78–2.77)	.23
Solid tumor size (cm)	2.49 (1.60–3.89)	<.001
MaxSUV	1.10 (1.04–1.17)	<.001
Multivariate analysis		
Solid tumor size (cm)	2.30 (1.46–3.63)	<.001
MaxSUV	1.08 (1.00–1.17)	.05

HR, Hazard ratio; *maxSUV,* maximum standardized uptake value.

variability in the SUVs obtained in the present study was minimized using an anthropomorphic body phantom. Therefore, quantitative SUVs adjusted by phantom studies can be quite dependable, and such correction will help to overcome a major limitation concerning the wide variability in SUVs among institutions in multicenter PET studies.

Generally, FDG uptake is dependent on tumor size,[19,20] and the present study demonstrated that solid tumor size was more closely related to the maxSUV than was the whole tumor size and that the solid tumor size is a potential marker of malignancy and prognosis. This finding is important for lung adenocarcinomas with a GGO component visualized on HRCT.

CONCLUSIONS

The predictive values of the solid tumor size visualized on HRCT and the maxSUV on PET/CT for pathologic high-grade malignancy and prognosis in cases of clinical stage IA lung adenocarcinoma were greater than those of whole tumor size. We recommend that the solid tumor size be used to determine the T descriptor in the TNM classification of lung cancer and should be defined as the true tumor size in cases of lung adenocarcinoma with a GGO component visualized on HRCT.

References

1. Okada M, Koike T, Higashiyama M, Yamato Y, Kodama K, Tsubota N. Radical sublobar resection for small-sized non-small cell lung cancer: a multicenter study. *J Thorac Cardiovasc Surg.* 2006;132:769-75.
2. Nakayama H, Yamada K, Saito H, Oshita F, Ito H, Kameda Y, et al. Sublobar resection for patients with peripheral small adenocarcinomas of the lung: surgical outcome is associated with features on computed tomographic imaging. *Ann Thorac Surg.* 2007;84:1675-9.
3. Nakata M, Saeki H, Takata I, Segawa Y, Mogami H, Mandai K, et al. Focal ground-glass opacity detected by low-dose helical CT. *Chest.* 2002;121:1464-7.
4. Jang HJ, Lee KS, Kwon OJ, Rhee CH, Shim YM, Han J. Bronchioloalveolar carcinoma: focal area of ground-glass attenuation at thin-section CT as an early sign. *Radiology.* 1996;199:485-8.
5. Noguchi M, Morikawa A, Kawasaki M, Matsuno Y, Yamada T, Hirohashi S, et al. Small adenocarcinoma of the lung: histologic characteristics and prognosis. *Cancer.* 1995;75:2844-52.
6. Goldstraw P, Crowley J, Chansky K, Giroux DJ, Groome PA, Rami-Porta R, et al., International Association for the Study of Lung Cancer International Staging Committee; Participating Institutions. The IASLC Lung Cancer Staging Project: proposals for the revision of the TNM stage groupings in the forthcoming (seventh) edition of the *TNM Classification of Malignant Tumours. J Thorac Oncol.* 2007;2:706-14.
7. Delbeke D, Coleman RE, Guiberteau MJ, Brown ML, Royal HD, Siegel BA, et al. Procedure guideline for tumor imaging with 18F-FDG PET/CT 1.0. *J Nucl Med.* 2006;47:885-95.
8. Nakayama H, Okumura S, Daisaki H, Kato Y, Uehara H, Adachi S, et al. Value of integrated positron emission tomography revised using a phantom study to evaluate malignancy grade of lung adenocarcinoma. *Cancer.* 2010;116:3170-7.
9. Okada M, Nakayama H, Okumura S, Daisaki H, Adachi S, Yoshimura M, et al. Multicenter analysis of high-resolution computed tomography and positron emission tomography/computed tomography findings to choose therapeutic strategies for clinical stage IA lung adenocarcinoma. *J Thorac Cardiovasc Surg.* 2011;141:1384-91.
10. Suzuki K, Kusumoto M, Watanabe S, Tsuchiya R, Asamura H. Radiologic classification of small adenocarcinoma of the lung: radiologic-pathologic correlation and its prognostic impact. *Ann Thorac Surg.* 2006;81:413-9.
11. Rami-Porta R, Ball D, Crowley J, Giroux DJ, Jett J, Travis WD, et al. The IASLC lung cancer staging project: proposals for the revision of the T descriptors in the forthcoming (seventh) edition of the TNM classification for lung cancer. *J Thorac Oncol.* 2007;2:593-602.
12. Aoki T, Tomoda Y, Watanabe H, Nakata H, Kasai T, Hashimoto H, et al. Peripheral lung adenocarcinoma: correlation of thin-section CT findings with histologic prognostic factors and survival. *Radiology.* 2001;220:803-9.
13. Takashima S, Maruyama Y, Hasegawa M, Yamanda T, Honda T, Kadoya M, et al. Prognostic significance of high-resolution CT findings in small peripheral adenocarcinoma of the lung: a retrospective study on 64 patients. *Lung Cancer.* 2002; 36:289-95.
14. Suzuki K, Asamura H, Kusumoto M, Kondo H, Tsuchiya R. "Early" peripheral lung cancer: prognostic significance of ground glass opacity on thin-section computed tomographic scan. *Ann Thorac Surg.* 2002;74:1635-9.
15. Ohde Y, Nagai K, Yoshida J, Nishimura M, Takahashi K, Suzuki K, et al. The proportion of consolidation to ground-glass opacity on high resolution CT is a good predictor for distinguishing the population of non-invasive peripheral adenocarcinoma. *Lung Cancer.* 2003;42:303-10.
16. Suzuki K, Koike T, Asakawa T, Kusumoto M, Asamura H, Nagai K, et al. A prospective radiological study of thin-section computed tomography to predict pathological noninvasiveness in peripheral clinical IA lung cancer (Japan Clinical Oncology Group 0201). *J Thorac Oncol.* 2011;6:751-6.
17. Okada M, Tauchi S, Iwanaga K, Mimura T, Kitaura Y, Watanabe H, et al. Associations among bronchioloalveolar carcinoma components, positron emission tomographic findings, and malignant behavior in small lung adenocarcinomas. *J Thorac Cardiovasc Surg.* 2007;133:1448-54.
18. Tsutani Y, Miyata Y, Misumi K, Ikeda T, Mimura T, Hihara J, et al. Difference in prognostic significance of maximum standardized uptake value on [18F]-fluoro-2-deoxyglucose positron emission tomography between adenocarcinoma and squamous cell carcinoma of the lung. *Jpn J Clin Oncol.* 2011;41:890-6.
19. Vansteenkiste JF, Stroobants SG, Dupont PJ, De Leyn PR, Verbeken EK, Deneffe GJ, et al. Prognostic importance of the standardized uptake value on (18)F-fluoro-2-deoxy-glucose-positron emission tomography scan in non-small-cell lung cancer: an analysis of 125 cases. Leuven Lung Cancer Group. *J Clin Oncol.* 1999;17:3201-6.
20. Downey RJ, Akhurst T, Gonen M, Vincent A, Bains MS, Larson S, et al. Preoperative F-18 fluorodeoxyglucose-positron emission tomography maximal standardized uptake value predicts survival after lung cancer resection. *J Clin Oncol.* 2004;22:3255-60.

Interactive CardioVascular and Thoracic Surgery 14 (2012) 5–11
doi:10.1093/icvts/ivr065 Advance Access publication 17 November 2011

INSTITUTIONAL REPORT

Radical hybrid video-assisted thoracic segmentectomy: long-term results of minimally invasive anatomical sublobar resection for treating lung cancer

Morihito Okada[a,*], Yasuhiro Tsutani[a], Takuhiro Ikeda[a], Keizo Misumi[a], Kotaro Matsumoto[a], Masahiro Yoshimura[b] and Yoshihiro Miyata[a]

[a] Department of Surgical Oncology, Research Institute for Radiation Biology and Medicine, Hiroshima University, Japan
[b] Department of Thoracic Surgery, Hyogo Cancer Center, Akashi, Hyogo, Japan

* Corresponding author. Tel: +81-82-2575869; fax: +81-82-2567109; e-mail: morihito@hiroshima-u.ac.jp (M. Okada).

Received 9 August 2011; received in revised form 28 September 2011; accepted 29 September 2011

Abstract

We analysed the results of radical segmentectomy achieved through a hybrid video-assisted thoracic surgery (VATS) approach that used both direct vision and television monitor visualization at a median follow-up of over 5 years. Between April 2004 and October 2010, 102 consecutive patients able to tolerate lobectomy to treat clinical T1N0M0 non-small cell lung cancer (NSCLC) underwent hybrid VATS segmentectomy in which we used electrocautery without a stapler to divide the intersegmental plane detected by selective jet ventilation in addition to the path of the intersegmental veins. Curative resection was achieved in all patients. The median surgical duration and blood loss during the surgery were 129 min (range, 60–275 min) and 50 ml (range, 10–350 ml), respectively. The complication rate was 9.8% (10/102) with the most frequent being prolonged air leak, and there was no case of in-hospital death or 30-day mortality post procedure. Five and seven patients developed locoregional and distant recurrences, respectively. The overall and disease-free 5-year survival rates were 89.8% and 84.7%, respectively. Radical hybrid VATS segmentectomy including atypical resection of (sub)segments is a useful option for clinical stage-I NSCLC. The exact identification of anatomical intersegmental plane followed by dissection using electrocautery is critical from oncological and functional perspectives.

Keywords: Segmentectomy • Lung cancer • Video-assisted thoracic surgery • Sublobar resection

THORACIC ONCOLOGIC

INTRODUCTION

Advances in radiographic devices such as high-resolution computed tomography (CT) and the widespread practice of low-dose helical CT for screening have resulted in an extraordinary increase in the early detection of ever smaller non-small cell lung cancers (NSCLCs), such as bronchioloalveolar carcinoma, that might possibly have more indolent biological behaviour. This trend has rapidly changed clinical practice in thoracic surgery, and thus concern has arisen over unified strategies that include whole lobectomy to treat small peripheral cancers. Removing a relatively large volume of healthy lung tissue could result in a poorer quality of postoperative life, a higher frequency of operative morbidity and a decreased likelihood of having a second or even a third NSCLC resected, for which such patients would survive long enough to become at risk. We have therefore actively performed radical segmentectomy with lymph node assessment not only for high-risk but also for good-risk patients with small clinical stage-I NSCLC [1–4]. The outcomes of the randomized study conducted by the Lung Cancer Study Group demonstrated that sublobar resections including wedge resections resulted in a higher rate of local recurrence compared with lobectomy in patients with clinical T1N0M0 NSCLC [5]. Thus, the incidence of non-anatomical stapled wedge resection has escalated and many recent residency programs in thoracic surgery do not cover segmentectomy as a mandatory procedure. However, we and other expert surgeons perceive segmentectomy as a crucial basic technique that should be mastered by all thoracic surgeons [6, 7].

We previously reported a novel segmentectomy in which the intersegmental plane was identified using selective jet ventilation under bronchofiberscopy [8]. Consequently, the segment to be removed can be inflated, whereas those to be preserved are maintained while deflated, which is contrary to the conventional procedure. However, this allows clear visualization of the anatomical intersegmental line between the segment to be resected and that to be preserved. The actual surgical margin in the inflated segment can be adequately grasped and a good surgical field can be obtained even through video-assisted thoracic surgery (VATS) without the need to physically suppress the other segments and lobes using an instrument. In addition, the anatomical intersegmental plane can be precisely dissected by electrocautery without any stapling. This allows the saved adjacent segments to remain completely expansive so that pulmonary function after surgery can be maximal.